D. Smittarello, V. Pinel, F. Maccaferri, S. Furst, E. Rivalta, V. Cayol, *Characterizing the physical properties of gelatin, a classic analog for the brittle elastic crust, insight from numerical modeling*, Tectonophysics, Volume 812, 2021, 228901.

The final published version is available online at: https://doi.org/10.1016/j.tecto.2021.228901

Graphical Abstract

Characterizing the physical properties of gelatin, a classic analog for the brittle elastic crust, insight from numerical modeling

Smittarello, D., Pinel, V., Maccaferri, F., Furst, S., Rivalta, E., Cayol, V.

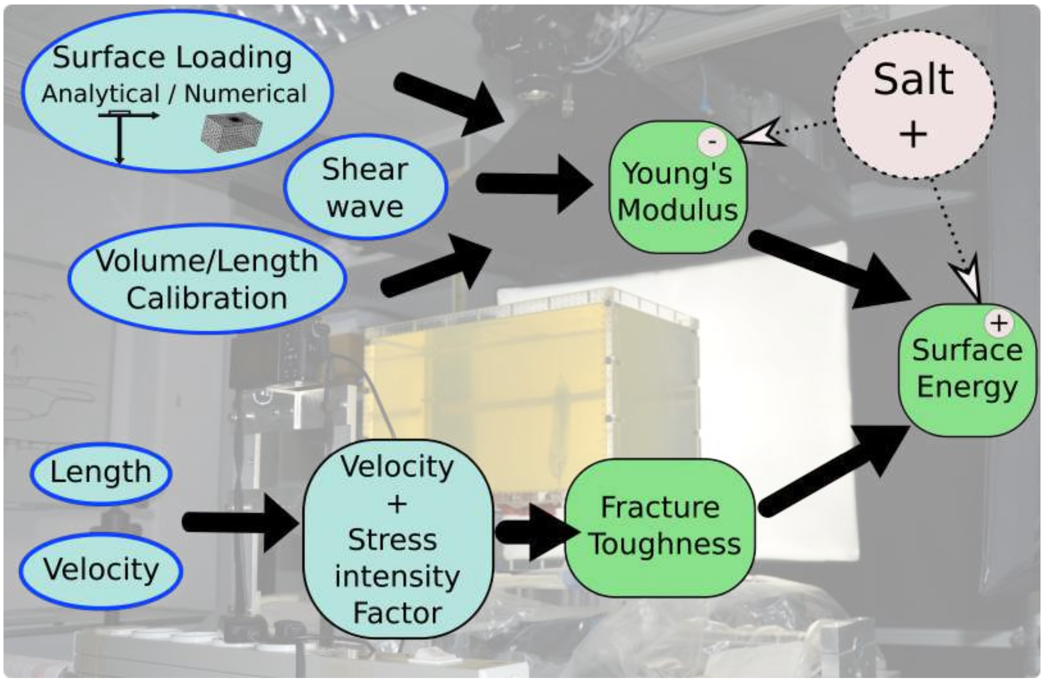

Highlights

Characterizing the physical properties of gelatin, a classic analog for the brittle elastic crust, insight from numerical modeling

Smittarello, D., Pinel, V., Maccaferri, F., Furst, S., Rivalta, E., Cayol, V.

- Numerical models improve the gelatin Young's modulus estimation by surface loading.
- Gelatin Young's modulus may be overestimated by 5 % when using an analytical solution.
- The gelatin Young's modulus can be derived from the length for an air-filled crack.
- Addition of salt to gelatin decreases its rigidity and increases its surface energy.

Characterizing the physical properties of gelatin, a classic analog for the brittle elastic crust, insight from numerical modeling

Smittarello, D.[a,c], Pinel, V.[a], Maccaferri, F.[b,d], Furst, S.[a], Rivalta, E.[b,e], Cayol, V.[f]

[a] *University Grenoble Alpes, University Savoie Mont Blanc, CNRS, IRD, UGE, ISTerre, Grenoble, France;*
[b] *Deutsches GeoForschungsZentrum GFZ, Section 2.1, Potsdam, Germany*
[c] *European Center for Geodynamics and Seismology, 19 rue Josy Welter, L-7256 Walferdange, Gd Duchy of Luxembourg;*
[d] *Istituto Nazionale di Geofisica e Vulcanologia, Sezione di Napoli - Osservatorio Vesuviano, Via Diocleziano 328, 80124, Napoli, Italy.*
[e] *Section of Geophysics, Department of Physics and Astronomy, Alma Mater Studiorum University of Bologna, Viale Berti Pichat 8, 40127 Bologna, Italy.*
[f] *Université Clermont Auvergne, CNRS, IRD, OPGC, Laboratoire Magmas et Volcans, F-63000 Clermont-Ferrand, France*

Abstract

Precise characterization of the mechanical properties of gelatin, a classic analog of the elastic crust, is necessary for scaling the mechanical models of the Earth's crust behavior in laboratory experiments. Here we reassess how to accurately calculate the Young modulus (E) of gelatin contained in experimental tanks. By means of dedicated analog experiments and finite element simulations, we estimate the bias introduced by using equations appropriate for a half-space to interpret the subsidence due to a cylindrical surface load applied on the gelatin. In the case of a standard experimental setup with gelatin adhering to the tank wall, we find E is overestimated by at least 5 % for a box with lateral size smaller than 20 times the cylinder diameter. In addition, we deduce a correction factor to be applied when using an analytical formula. We confirm that measuring the shear velocity leads to accurate estimates for the rigidity of gelatin. We also propose a new method for in situ Young's modulus estimation, relying on the length of air-filled propagating crack. Indeed, for a given injected volume, this length depends only on the density contrast between air and gelatin and on the Young's modulus of the gelatin. The fracture toughness of the gelatin is estimated independently. Direct comparison between fracture toughness and Young's modulus shows that for a given Young's modulus, salted gelatin has a higher fracture toughness than unsalted gelatin.

Keywords: Analog modeling, Gelatin, Young's modulus, Fracture toughness, Crack propagation

---

1. Introduction

Gelatin, a transparent animal-derived biopolymer in its sensu stricto appellation [1], has been used as an analog of the crust and lithosphere, in a wide range of laboratory experiments [2]. It has proven useful to study the seismic cycle in subduction zones [e.g. 3], the deformation of the upper crust around magma storage zones [e.g. 4, 5] or magma transport through either open conduits [e.g. 6] or magma-filled cracks [e.g. 7, 8, 4, 9, 10, 11, 12, 13]. A physical understanding of the Earth can be gained from analog experiments provided that they are geometrically, kinetically and dynamically scaled [14]. As a consequence the physical and rheological characterization of the gelatin has been addressed by numerous studies in Earth Sciences [e.g. 1, 15, 16] as a complement to work done in the food industry [e.g. 17].

Gelatin has been shown to behave in its gel-like state as a visco-elastic medium, which makes it particularly appropriate for tectonic studies [1]. The balance between the viscous and elastic behavior has been investigated by measuring the storage (G') and the loss (G") moduli over a broad range of deformation rates. This balance depends mainly on gelatin concentration, temperature and aging [1, 16, 15]. If prepared with a concentration between 2 and 5 wt %, gelatin behaves elastically at low temperatures (6-14°C) for time scales up to a few hours [1, 16, 15]. The main focus of the present study is the characterization of gelatin elastic behavior during fluid-filled crack propagation experiments, with application to the study of magma transport through the crust.

Elastic behavior of gelatin can be characterized by its Poisson's ratio ν and its Young's modulus E. Poisson's ratio of gelatin is generally assumed to be 0.5, which means that gelatin is incompressible [18, 19]. Slightly smaller Poisson's ratio with values around 0.45 for gelatin concentration greater than 3 wt % were measured by van Otterloo and Cruden [15] but the values they obtained for smaller concentration were unrealistic [15]. Pansino and Taisne

[20] inferred a value larger than 0.47 with a 2.7 wt % concentration. Because these values are very close to 0.5, we will further consider gelatin as an incompressible medium. In contrast, crustal rocks generally have a Poisson's ratio around 0.25.

The Young's modulus can be derived from the limit of the storage modulus G' when the frequency tends to infinity and thus measured on small samples of gelatin with a rheometer [1]. However this method is destructive and limited to a reduced size sample. The gelatin Young's modulus increases with the gelatin concentration and decreases with the temperature. It also depends on the gelatin composition, on the preparation protocol and on the cooling history [16]. It might sometimes be useful to add salt to the gelatin in order to slightly increase its density and improve the scaling in specific conditions [21, 22, 23]. In particular, when attempting to model viscous effects on magma propagation, the use of salted gelatin is required in order to guarantee a sufficient buoyancy of the oils injected inside the gelatin. Brizzi et al. [24] have shown that the addition of salt dramatically affects not only material behavior, but also gel structure stability. Adding salt induces a decrease of both the Young's modulus and the viscosity, an increase of the time required for cooling down to a stable state and it tends to promote the elastic behavior compared to the viscous one. They also noted that the transparency might be reduced by salt addition and that the mechanical properties become highly sensitive to the preparation protocol such that it is more difficult to control the reproducibility of the experiments. Due to the complex behavior of the gelatin and the variability of experimental conditions, it is recommended to quantify the Young's modulus associated with each gelatin tank, which requires the use of non destructive and *in situ* measurements.

The Young's modulus of crustal rocks can be measured in the laboratory by means of uniaxial strain-stress experiments [25]. However, interpolating laboratory measurements on small rock samples to infer the Young's modulus value at depth and the crustal behavior is not trivial. The main issues in laboratory experiments are related to the scaling and use of non-fractured samples at low pressure and temperature that may not reflect the "in situ" conditions at depth in the crust. There are basically two ways of quantifying the in-situ crustal Young's modulus: either using the surface displacement induced by surface loading or unloading events [26, 27, 28], often referred to as a "static" estimation, or using seismic wave velocities derived from local tomography surveys [29, 30], often referred to as "dynamic" estimation. A systematic discrepancy has been evidenced between the dynamic and static

Young's moduli. For rocks, the dynamic Young's modulus is always larger by a factor which depends on the porosity [31, 32].

For gelatin in a tank, the most commonly used in-situ and non-destructive method is based on surface loading. It consists of measuring the vertical displacement induced by a circular load applied at the surface and inverting for the Young's modulus using an analytic formula for a circular rigid load applied on an infinite half-space [e.g. 33, 11, 16, 34, 35]. Due to the assumption of an infinite medium, the diameter of the load should be smaller by a factor of ten than the smaller dimension of the tank (either vertically or laterally) [16].

However, gelatin tanks used for experiments are usually of limited size mainly to ensure a volume which is manageable to produce. It follows that instrumentalists always have to be cautious of boundary effects. One way to account for the rigid boundaries at the box walls consists in using numerical models to infer the actual state of stress within the gelatin [e.g. 11]. For instance, Corbi et al. [36] calculated the state of stress inside their gelatin tank using a 2D-axisymmetric Finite Element Model (FEM) in order to interpret the crack path observed in experiments. Pinel et al. [37] improved the estimate of the stress field acting within the gelatin tank previously used by Watanabe et al. [38] to quantify the influence of the external stress field on the fluid-filled crack path. This was done by computing the stress field induced by a surface load using a 3D numerical simulation, taking into account the geometry of the tank and the geometry of the load, and by comparing it to the analytical solution previously used. In the same way, Maccaferri et al. [13] computed both the local stress field and the surface displacement induced by a load of given size, accounting for the rigid boundaries of the box and used this information to obtain an accurate value of the Young's modulus for gelatin tanks.

More recently, Pansino and Taisne [39, 20] proposed to derive the Young's modulus from the propagation velocity of shear waves. They took advantage of gelatin being a birefringent photo-elastic material. Its refractive index varies with the stress applied such that, using a pair of polarizing filters enables to visualize the deviatoric stress and track the propagation of shear waves within the gelatin. This method can be thought of as the equivalent of crustal Young's modulus estimations from seismic waves. The results were compared with estimations made using the static loading method and showed to be in good agreement [20]. In addition, Pansino and Taisne [20] proposed that the shear wave method could potentially be used to quantify any variations of the Young's modulus inside the tank.

Experiments of fluid-filled crack propagation also require the characterization of the brittle behavior of the gelatin. A key parameter is the fracture toughness. Crack propagation will only occur once the stress intensity factor at the tip, which depends on the applied stress and the shape of the crack, exceeds the fracture toughness of the surrounding medium. The fracture toughness K_c is linked to the Young's modulus by the following equation expressed by Griffith [40]:

$$K_c = \sqrt{2\gamma_s E}, \tag{1}$$

with γ_s the surface energy of the solid, which for gelatin is estimated around 1.0 ± 0.2 J.m^{-2} [33, 16]. This relationship is often used to derive the fracture toughness but it should be kept in mind that the value of γ_s is expected to depend on the gelatin composition and might be different when salt is added [22]. Alternatively, the fracture toughness can be quantified by measuring the pressure required to propagate a pre-existing fluid-filled crack [33, 16]. Another method consists in retrieving the stress intensity factor of propagating cracks for various velocities of propagation: the fracture toughness is then given by the limit of the stress intensity factor when the propagation velocity tends to zero [41].

In the current study, we further detail how numerical simulations may improve the determination of gelatin Young's modulus by surface loading. In particular, we provide an accurate estimate of the error resulting from using the analytical formula when deriving the Young's modulus by surface loading. We also compare Young's modulus obtained by surface loading to values derived by the shear wave velocity method. Then, Young's modulus estimates are used to derive a calibration of the relation between the injected volume and the crack length in case of air-filled cracks. We thus provide a new method for Young's modulus estimation. Finally, we characterize the fracture toughness of the gelatin to quantify the effects of adding salt to gelatin on its brittle behavior.

2. Methods

2.1. Laboratory technique

Table 1: Gelatin properties for the 37 tanks. E_{an}^{load} is calculated only when a circular load was applied to the surface with Eq. 5 whereas E_{num}^{load} is calculated with the Finite Element model with the rigid load condition taking into account the exact geometry of the load applied. Injections is for the number of injections performed and used in this study.

Tank number	**Tank geometry**	**Height (cm)**	**Volume (L)**	**Gel. (%)**	**Salt (%)**	ρ_{gel} **kg.m^{-3}**	**T$_{gel}$** (°C)	**Duration** (h)	**Injections** (.)	**E$_{an}^{load}$± std (Pa)**	**E$_{num}^{load}$± std (Pa)**	**Shear velocity ± std (cm/s)**	**E^{shw}± std (Pa)**	**K$_c^{2D}$ Pa.m$^{1/2}$**	**K$_c^{3D}$ Pa.m$^{1/2}$**
1701	big	20.00	16.00	2	0	1020		1.6	11		1637 ± 27			49	54
1702	big	20.00	16.00	2	0	1020		1.7	9		2277 ± 136			51	56
1703	big	20.00	16.00	2	0	1020		1.1	7		2315 ± 118			58	64
1704	big	20.00	16.00	2	0	1020		1.8	6		2312 ± 105			48	53
1705	big	20.00	16.00	2	0	1020		2.1	8		2408 ± 354			54	60
1706	big	20.00	16.00	2	0	1020		1.6	7		2286 ± 142			48	53
1707	big	20.00	16.00	2	0	1020		1.6	7		2342 ± 276			52	58
1708	big	20.00	16.00	2	0	1020		1.3	6		2117 ± 130			44	48
1801	big	9.62	7.70	2.5	11	1080		1.8	5		1308				
1802	big	22.00	17.60	3	10	1060		3.3	4		2001 ± 174				
1803	big	22.65	18.12	3.5	15	1120		2.9	6		630				
1804	big	22.71	18.17	3.5	15	1120		4.4	7		2201 ± 352			66	73
1805	big	21.81	17.45	3.5	15	1120		3.8	6		834 ± 128				
1806	big	23.00	18.40	3.5	15	1120		4.0	7		966 ± 121			42	47
1807	big	22.30	17.84	3.5	15	1120		5.2	7		845 ± 257			41	45
1808	big	21.92	17.54	3.5	15	1120		3.5	4		909 ± 98				
1809	big	22.32	17.86	3.5	15	1120		4.0	8		800 ± 101				
1810	big	21.96	17.57	3.5	15	1120		2.5	4		938 ± 100				
1901	big	12.06	9.65	2	0	1020	10	0.4	7		2201			56	62
1902	big	18.76	15.01	2	0	1020	?-12	0.2	7		1937			57	62
1903	big	18.81	15.05	2	0	1020	?-12	1.1	9		2085			59	65
1904	big	19.19	15.35	2	0	1020		0.8	7		1885	54.32 ± 3.54	903 ± 11.52		
1905	big	15.88	12.70	3.5	15	1120		1.6	5		1995	61.46 ± 10.89	1269 ± 40.16		
1906	big	13.05	10.44	3.5	15	1120		2.1	5	1769 ± 94	1443 ± 77	65.97 ± 7.14	1462 ± 28.27	74	82
1907	small	22.56	4.36	2.5	15	1120		0.5	1	1783 ± 55	1290 ± 40	64.73 ± 5.00	1408 ± 19.43		
1908	cylinder	26.18	4.20	3.5	15	1120	10	1.7	1	3649 ± 297	2892 ± 236	98.07 ± 13.11	3232 ± 77.15		
1909	big	21.92	17.54	2	15	1120	14	2.9	8		306 ± 61	17.25 ± 2.53	100 ± 2.618	17	19
1910	small	23.09	4.46	1.5	15	1120	8	0.4	1	1532 ± 477	846 ± 263	34.71 ± 2.30	405 ± 4.78		
1911	cylinder	25.66	4.12	1.5	15	1120	8-11	1.7	3	700 ± 50	441 ± 32	34.86 ± 3.34	408 ± 6.99		
1913	big	21.37	17.10	2	15	1120	14	2.1	5		597 ± 47	22.64 ± 2.39	172 ± 3.25		
1914	small	21.53	4.16	2	15	1120	8-12	0.8	1	1382 ± 137	762 ± 76	46.72 ± 2.00	733 ± 5.62		
1915	cylinder	28.81	4.63	2	15	1120	8-14	0.7	3	1500 ± 265	950 ± 168	59.20 ± 2.70	1177 ± 9.59		
1916	big	21.53	17.22	2	15	1120	14	3.5	12		595 ± 19	25.14 ± 2.71	212 ± 4.09	30	33
2002	big	22.50	18.00	1.8	0	1020	5.2-7.2	1.5	7		1847 ± 20			51	57
2003	big	22.50	18.00	1.6	0	1020	10.2-13.3	1	10		1005 ± 20			36	40
2004	big	22.50	18.00	1.5	0	1020	8.2-13.3	1	9		1113 ± 16			38	42
2005	big	22.50	18.00	2	15	1120		1	9		666 ± 16			33	37

2.1.1. *Gelatin preparation*

We used type A pig-skin gelatin (Bloom number 280g) purchased from Italgelatine S.p.A., in the form of solid granules. Gelatin with different concentrations were prepared and salt was added to some preparations in order to increase the gelatin density. In total we made 37 tanks of gelatin, 15 at 1.5 to 2 wt % without adding salt and 22 varying the gelatin concentration from 1.5 wt % to 3.5 wt % and the salt concentration from 10 to 15 wt % (Tab. 1).

To prepare the unsalted gelatin, we completely dissolved the granules of gelatin with hot water ($\sim 60°$C). In order to get a transparent solid, a perfect dissolution of the gelatin granules is required. We proceeded in several steps, dissolving only a fraction of the total mass needed to prepare one tank in a 2 L beaker and holding the solution on warm plate at 60°C. When all the granules were dissolved we diluted with warm water to reach the desired volume and concentration. We let it cool down to room temperature for a few hours. When the preparation had reached $\sim$32°C, we mixed it to homogenize the gelatin and we transferred the liquid gelatin into the tank, before placing it into the refrigerator at $\sim$8° C for 20 hours. According to Kavanagh et al. [16] and van Otterloo and Cruden [15] liquid gelatin solidifies, behaving as a visco-plastic solid below 25°C and as an elastic solid below 15°C. Note that during the preparation, the temperature of the gelatin should never exceed 70°C or drop below 4°C to avoid the denaturation of the peptide chains by heating or freezing, respectively [1]. Following Brizzi et al. [24]'s protocol, in order to add salt to the recipe, we first dissolved the salt in hot water, then we used the salty water to dissolve the gelatin granules, as previously described. It is important to first dissolve the salt and then the gelatin granules to avoid the precipitation of the peptide chains and to preserve the transparency of the solid.

To prevent the formation of a tough "skin" on the gelatin surface caused by water evaporation, a thin layer of vegetable oil was poured on top of the gelatin (salted and unsalted) before placing it into the fridge. The oil was removed before starting the experiments.

The gelatin density was computed as the ratio between its mass and the volume. Using a graduated cylinder, we measured a volume of 50$\pm$1 mL of liquid gelatin and weight it with a gram-accurate scale. Density of unsalted and salted (15 wt %) gelatin were estimated to 1020$\pm$40 kg.m^{-3} and 1120$\pm$40 kg.m^{-3}, respectively. Although, we have a quite large formal absolute error due to the poor scale resolution, we obtain very good reproducibility in our measurements from one tank to another. We checked that density changes due to cooling and solidification were negligible by repeating density measurements at different temperatures, and checking that the gelatin level in the tank did not change after solidification.

2.1.2. Experimental setup and recordings

We used three different plexiglas tanks: a cylindrical one with a diameter of 14.3 cm and a height of 30 cm and two cuboids with dimensions $L \times l \times H$ of 13.9 cm$\times$13.9 cm$\times$24 cm for the smaller one and 40 cm$\times$20 cm$\times$25 cm for the larger one. The larger tank corresponds to the one used for experiments described by Maccaferri et al. [13] (see Fig. 1). The height of gelatin was usually close to 20 cm (see Tab. 1). For experiments 2002, 2003 and 2004, both the room and the gelatin temperature were continuously recorded during the whole duration of the experiment by thermocouples, whereas for some other experiments the gelatin temperature was measured by an infrared thermometer. However, we do not have temperature records for all the experiments: when available the gelatin temperature, or temperature values for the beginning and the end of the experiment are given in Tab. 1 together with the duration of the whole experiment.

In order to measure the gelatin Young's modulus by static deformation, the gelatin surface was loaded with rectangular (6$\times$14 cm) or circular shapes (with diameters ranging from 2 to 4 cm) and masses ranging from 3 g to 331 g. With the corresponding pressure range, we induced surface displacement large enough to be accurately measured, without damaging the gelatin. We used a digital caliper, whose accuracy is 10^{-2} mm, to measure the subsidence. We fixed the caliper to a rigid support on the top of the tank (Fig. 1c). We measured the distance to the gelatin surface without load d_1 and the distance to the top of the load d_2. Knowing the load thickness e, we can derive the vertical surface displacement u induced by the load (Eq. 2):

$$u = d_2 + e - d_1 \tag{2}$$

The main limitation to the measurement accuracy comes from the ability of experimentalists to use the caliper without deforming the gelatin surface while measuring the subsidence. To reduce the uncertainties, we repeated the measurements for each tank at least three times using the same load until getting 3 values less than 0.2 mm apart, and when possible, we used several loads with increasing mass.

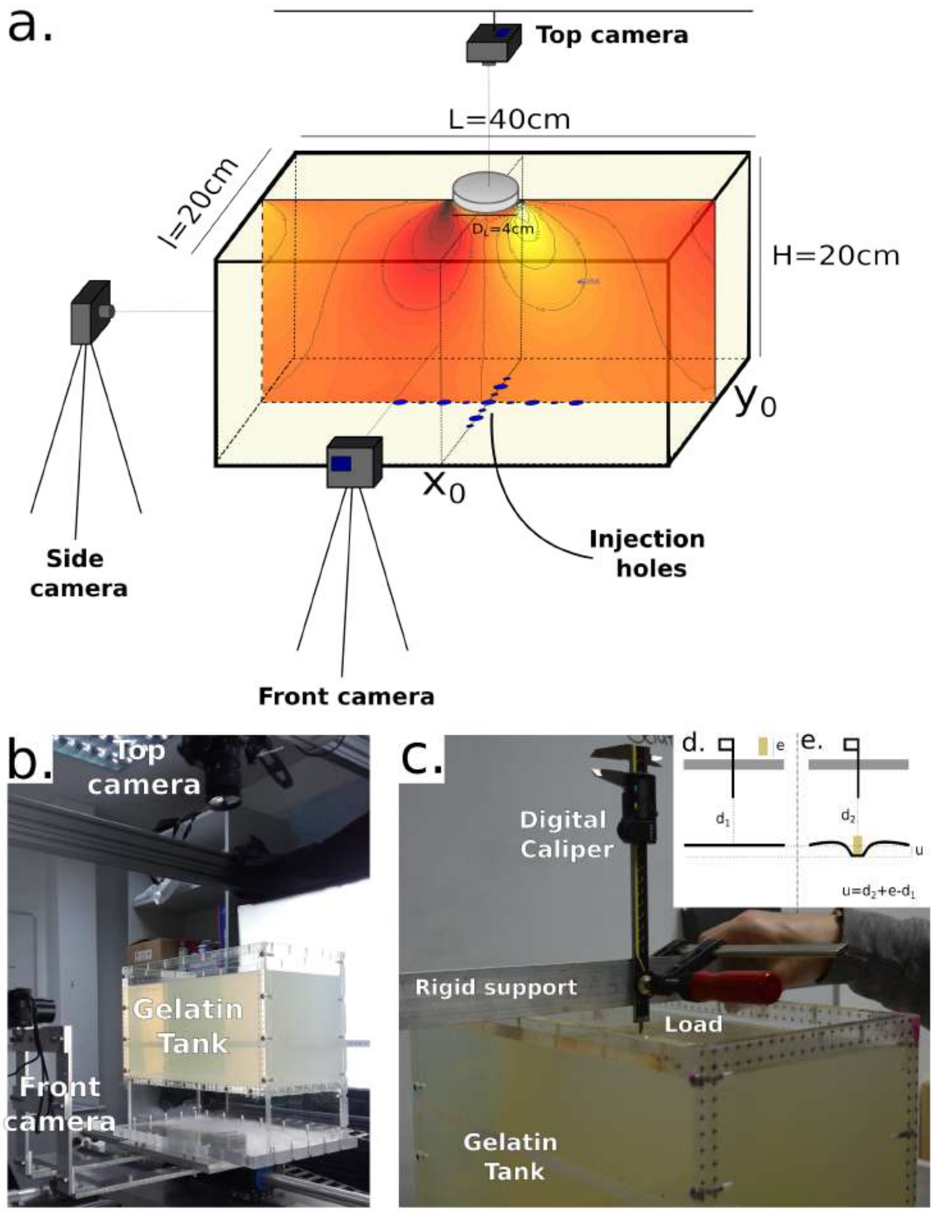

Figure 1: Experimental set-up. (a) Sketch of the experimental set-up and location of the three cameras. Section along plane $y = 0$ shows shear stress induced by the loading (grey cylinder). The 15 injection holes (2 sizes) are marked by blue circles on the underside of the tank. (b) Photography of the experimental set-up. Two lamps illuminate the tank from the back and right sides through the white screens. (c) Photography of the measurement of the surface vertical downward displacement induced by a load applied at the surface. Inset diagrams schematize the two steps of a measurement (d) measuring the reference distance d_1 before putting the load and (e) measuring the distance d_2 to the top of the load of known thickness e.

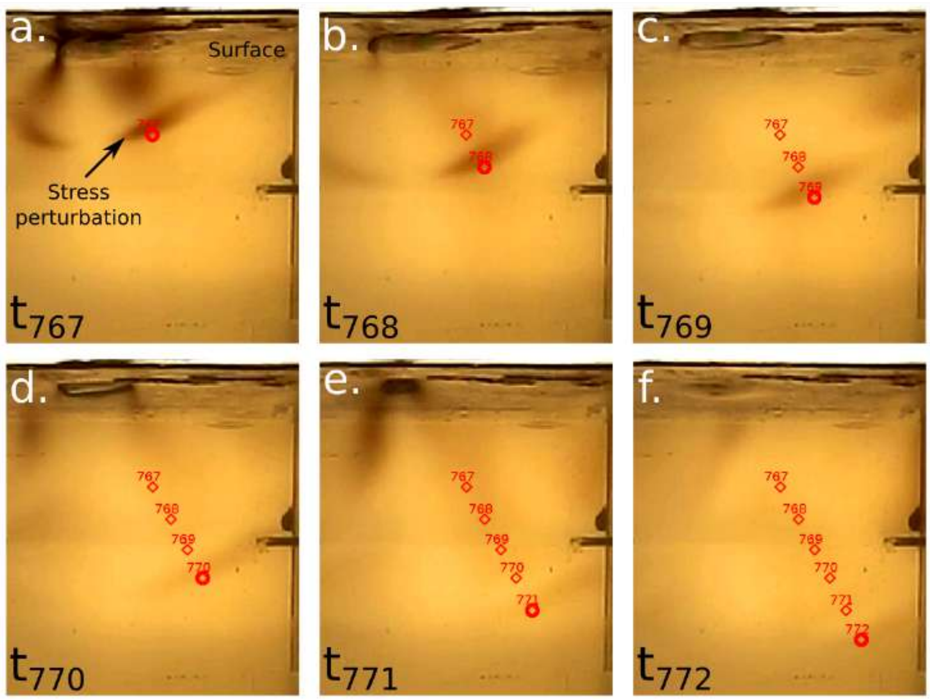

Figure 2: Shear wave velocity measurements with TRACKER. Panels (a to f) display screenshot of six successive images (t_{767} to t_{772}) from the video records of tank 1910 showing shear wave propagation front after exciting the surface. Red dots indicate the manual picking of the propagation front position to compute the velocity. Note that the shear wave attenuates quickly and it becomes increasingly difficult to track it manually.

In order to estimate the gelatin Young's modulus by measuring the shear-waves propagation velocity, we added polarizing filters on both the front and back sides of the tank. Following Pansino and Taisne [39, 20], we excited the gelatin surface with a spoon, and we recorded the shear wave propagation with the front camera. Using the open source software TRACKER [12], we measured the propagation velocity (Fig. 2). For each tank, we performed velocity measurements on several wave trains by manually picking the propagation front on at least 4 to 5 successive images. Then we computed the mean velocity and the standard deviation associated to each tank.

In order to study the fluid-filled crack propagation, we used a syringe to inject a finite volume of air from some holes at the bottom of the tank. The fracture orientation was controlled by carefully orienting the needle used for the injection. No slit was needed, we let the air create its own fracture. On the bottom of the larger rectangular tank, 15 holes with 2 cm in between allow to perform several injections into the same gelatin. Three perpendicular cameras recorded the fluid-filled crack shape and path. Two spotlights illuminated the tank from the back and right sides (Fig. 1). Videos subsampling was done with the video editing and open source software Shotcut [42]. The software TRACKER was used to measure the length L' of the air-filled cracks and to extract the path and the velocity of the crack. When all injections were completed in a tank, we took several pictures of a ruler at the location of the cracks in order to measure the calibration factor F needed to scale the videos. The crack length L was computed as $L = F \times L'$. Thus, the statistical error on the crack length is given by:

$$\frac{\sigma_L}{L} = \sqrt{\left(\frac{\sigma_F}{F}\right)^2 + \left(\frac{\sigma_{L'}}{L'}\right)^2} \tag{3}$$

Where σ is the standard deviation. Given that $\frac{\sigma_F}{F} = 0.024$ and $\frac{\sigma_{L'}}{L'} = 0.026$, we obtain $\frac{\sigma_L}{L}$=0.035.

2.2. Numerical simulations

In order to take into account the finite size of the tank and the exact shape and size of the circular load, we use a 3D FEM to compute the surface displacement induced by the applied load. Numerical simulations are performed with the commercial software COMSOL [43] applying a zero displacement condition to the lateral and bottom boundaries of the gelatin to reproduce the adherence of the gelatin to the tank walls. We use a mesh made of about 330,000 tetrahedral units, refined in a vertical plane centered below the load as well as on the upper surface around the load (minimum size of the mesh was set to 2 mm). The upper surface is considered as a free surface except where the load is applied. To simulate the loading, the easiest boundary condition to be considered would be a constant pressure

$$P_{Load} = \frac{4 m_L g}{\pi D_L} \tag{4}$$

with g the standard acceleration due to gravity and m_L the load mass applied on the circular surface of diameter D_L (Fig. 3a). We will refer to this condition, as the "uniform pressure condition". However, this boundary condition is not fully satisfactory as rigid loads are applied to the surface inducing a uniform vertical displacement below the load. To better reproduce this

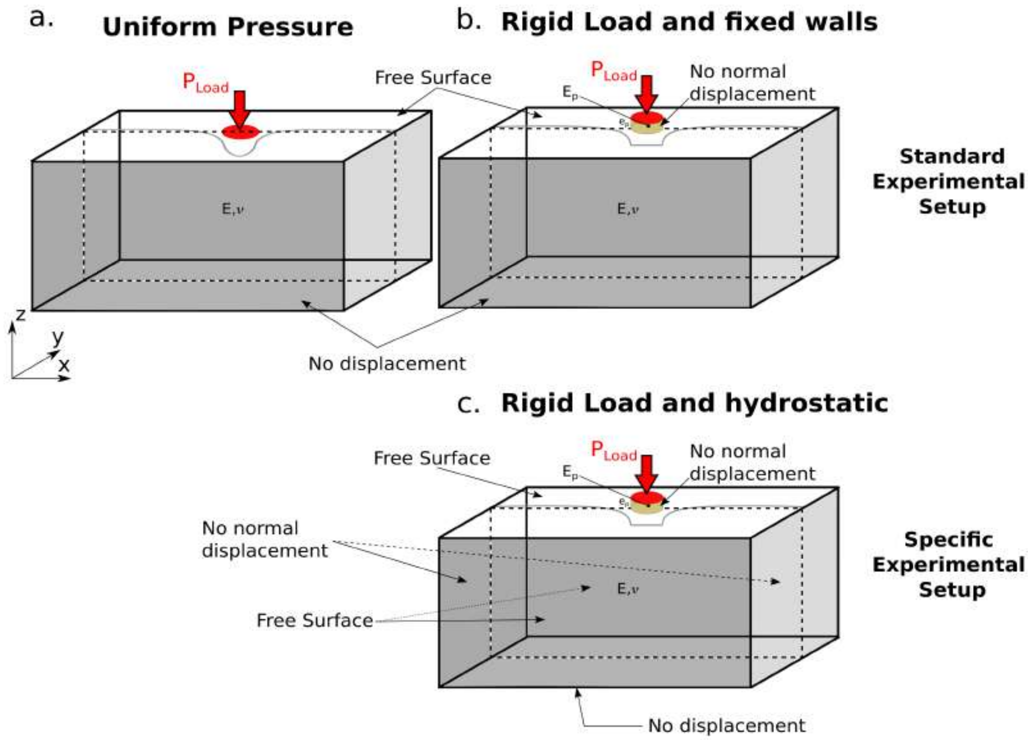

Figure 3: Boundary conditions applied in the numerical model and modeled surface displacements. The gray line shows the shape of the vertical component of the surface displacement induced by the boundary condition applied to the surface: (a) uniform pressure with gelatin adhering to the tank walls, (b) rigid load with gelatin adhering to the tank walls and (c) rigid load with gelatin in contact with water on two of the lateral sides of the gelatin block.

condition we simulate a thin (thickness e_p) rigid plate characterized by a large Young's modulus E_p. On the upper surface of this plate we apply the pressure P_{Load}. We also apply a condition of zero horizontal displacement to the lateral edge of this rigid plate (Fig. 3b). We will refer to this condition as the "rigid load condition". We set the values of E_p and e_p to 10^9 Pa and 4 mm respectively, to ensure a uniform vertical displacement below the applied load. As a theoretical value of 0.5 for the Poisson's ratio cannot be handled numerically, we set it to 0.49.

We compare the simulations using constant pressure and rigid load in similar conditions. We also run a set of simulations for a given load, increasing the box size.

Additionally, several studies [34, 44], have presented an experimental setup where gelatin is in contact with water on two lateral sides and detached from the other two sides of the tank. In order to discuss the influence of such a specific setup, we also applied another set of lateral conditions with a free surface on the two proximal lateral sides and a roller condition (zero displacement in the direction perpendicular to the tank wall) on the distal lateral sides (Fig. 3c).

3. Young's modulus determination by surface loading

3.1. Validity domain of the analytical solution

The relationship between the vertical surface displacement (U_z) beneath a rigid load of mass m_L applied to the surface of a half-space is given by the analytical formula (see Timoshenko et al. [45]):

$$U_z = \frac{m_L g(1-\nu^2)}{D_L E}, \tag{5}$$

where D_L is the load diameter. This method has been followed by most analog modelers to estimate the Young's Modulus of gelatin [e.g. 33, 11, 16, 34, 35]. However, assuming an infinite half space, such formula may introduce an error. This error was reported to remain small providing that the tank minimum size is ten times larger that the load diameter [16]. This estimation was derived from a correlation study between the Young's modulus estimate and the ratio of the load versus tank dimensions [16]. As the tank size is usually limited for practical reasons, this condition might be difficult to fulfill, in particular, because the load applied should be large enough to ensure significant displacement and it should be applied over an area large enough to avoid damaging the gelatin. In our case, even with our largest cuboid tank, the tank minimum dimension is indeed only five times larger than the load we applied. In order to quantify the error performed when using Eq. 5 as a function of the tank size, we compare the surface displacement calculated from the numerical simulation with the one predicted by the analytical formula.

Numerically, we apply a circular load (mass $m = 8$ g and diameter $D_L = 40.04$ mm) to the center of our largest rectangular tank and we progressively multiply the tank size by a factor f up to 80. Calculations are done both for the uniform pressure condition (Fig. 3a) and the rigid load condition (Fig. 3b) with gelatin adhering to the tank walls. The gelatin Young's modulus is set to 1000 Pa. Displacement profiles are shown in Fig. 4. As expected, the uniform pressure solution (dashed lines in Fig. 4) results in a maximum displacement below the load center while the rigid load condition produces a smaller and uniform displacement below the load which better reproduces our experimental conditions. We also represent the analytical solution for a uniform pressure load, which can be derived from Sneddon [46] as proposed by Sigmundsson and Einarsson [47] and Pinel et al. [28]:

$$U_z = \frac{4}{\pi}\frac{m_L g(1-\nu^2)}{D_L E} \tag{6}$$

We find that using a uniform pressure (Eq. 6) instead of a rigid load (Eq. 5) as boundary condition for the loading, would produce an overestimate of the Young's modulus E by a factor $4/\pi \sim 1.27$ for an infinite half-space. Moreover, both analytical formulas (Eq. 5 and 6) predict more vertical displacement than the corresponding numerical solution. Therefore, if such formula is applied to our largest cuboid tank (Tab. 2), E gets overestimated by 15% and 21% for the uniform pressure and the rigid load conditions, respectively.

In Tab. 2, displacements at the center of the load are also estimated using analytical formulas and a Poisson's ratio value of 0.49 (instead of 0.5) similarly to numerical simulations. Using a Poisson's ratio of 0.49 for the rigid load condition (Eq. 5) produces an overestimate of the vertical displacement by 1% (0.02mm). Such an overestimate is negligible in comparison to the error made by ignoring the boundary effect.

Both Fig. 4 and Tab. 2 show that when the tank size increases, numerical solutions tend to the value given by the analytical ones, which confirms the validity of the numerical model.

We compare the estimation of the Young's modulus when using the analytical formula (Eq. 5) to the numerical solution for the rigid load conditions (Tab. 2) as a function of the relative size of the load and the tank (Fig. 5). The caliper we used to measure the subsidence has an accuracy of 0.01 mm which corresponds to an error of 5% on the Young modulus estimate. According to Fig. 5, the ratio between the shortest dimension of the tank and the load diameter must be at least 21 for the error being less than 5% in the case of an experimental setup with gelatin adhering to the tank walls. This ratio is twice larger than the ratio previously recommended based on correlation studies [16]. For ratios below twenty, side effects due to the rigid walls of the tank cannot be neglected and the analytical formula significantly overestimates the displacement induced by a given load thus producing an overestimation of the Young's modulus of the gelatin (see also Tab. 1). Fig. 5 also shows that, when a specific experimental setup that ensures hydrostatic conditions on the proximal lateral sides of the gelatin block is used, the use of the analytical solution is less problematic. Then the analytical solution can be used provided that the shortest dimension of the tank remains 7 times larger than the load diameter. However even in the few studies that consider these specific lateral conditions, the Young's modulus was measured before the gelatin sides were melted and replaced by water meaning that the gelatin adhered to wall during the Young's modulus measurement. While most experimenters indicate the size of the tank they are using, the size of the load applied during the Young's modulus measurement is never provided except by Kavanagh et al. [16]. In the literature, the minimum size of the tank ranges from 8.6 cm [16] to 80 cm [6], which means that the maximum size of the applied load should be less than 0.4 cm for the smallest tanks and less than 3.8 cm for the largest. We provide a solution to this problem as from our results, it is possible to derive a correction factor to be applied to the value derived using the analytical formula in order to take into account the actual size of the tank (Fig. 5) and thus obtain a reliable value for the Young's modulus.

3.2. Young's modulus estimations by surface loading

Based on the results presented in the previous paragraph, the best method to estimate the Young's modulus by surface loading is to use the numerical simulation with a rigid load condition. We thus follow this strategy. Using the FEM simulation, with a geometry corresponding to each tank and each load considered, we compute the surface displacement U_z^{FEM} induced by the load with a Young's modulus value of E^{FEM} =1000 Pa, Poisson's ratio ν =0.49 and gravity $g = 9.81$ m.s^{-2}. For each measurement of surface subsidence in the analog setup U_z^{mes}, we can determine a Young's modulus value E^{load} using the following equation:

$$E^{load} = \frac{E^{FEM} U_z^{FEM}}{U_z^{mes}} \tag{7}$$

The Young's modulus is estimated for the 37 gelatin blocks (15 tanks filled with unsalted gelatin at 1.5 to 2 wt % and 22 tanks filled with salted gelatin at 1.5 to 3.5 wt % of gelatin and 10 to 15 wt % of salt). We estimate a value

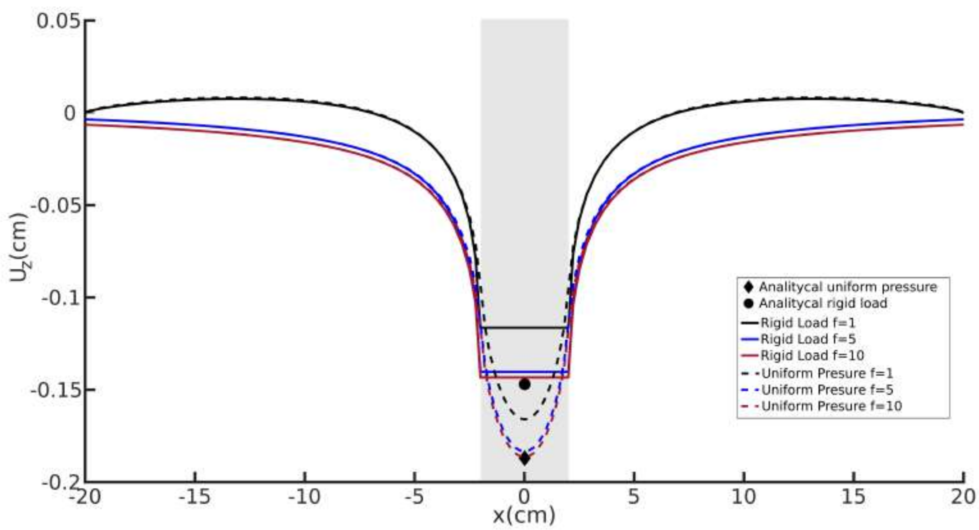

Figure 4: Profile of vertical surface displacement along x-axis (y=0, profile at the load center) for a circular load (diameter D_L = 40.04 mm, mass m_L = 8 g) applied to the surface of a rectangular tank (dimensions L×l×H of 40 cm×20 cm×20 cm multiplied by a factor f, the value $f = 1$ corresponding to the largest rectangular tank we used in our experiments). The Young's modulus is set to 1000 Pa. Black, blue and red solid lines are profiles calculated with the FEM for, respectively $f = 1$, $f = 5$ and $f = 10$. Dashed lines are for solutions derived with the uniform pressure condition, whereas plain lines are for solutions derived with the rigid load condition (in the case of the experimental setup with gelatin adhering the tank walls). Black diamond and circle represent the vertical displacement from analytical formulas (in x=0 at the load center) considering, the uniform pressure and the rigid load condition, respectively.

Table 2: Comparison of modeled vertical displacement induced by a circular load (diameter $D_L = 40.04$ mm, mass $m_L = 8$ g) applied at the surface of a rectangular tank (dimensions L×l×H of 40 cm×20 cm×20 cm multiplied by a factor f, the value $f = 1$ corresponding to the largest rectangular tank we used in our experiments). The Young's modulus is set to 1000 Pa. Two analytical solutions are tested also with three numerical solutions ("uniform pressure condition" with gelatin adhering to the walls of the tank, "rigid load condition" with gelatin adhering to the walls of the tank and "rigid load condition" with gelatin in contact with water on two of the lateral sides of the gelatin block) for several values of the tank size. In numerical simulations, the Poisson's ratio value is set to 0.49. FEM: Finite Element Model ; P: uniform pressure ; rgdL: rigid load; Swall: gelatin adhering to the tank walls; Fwall: gelatin in contact with water on two of the lateral sides of the gelatin block.

Model		**Tank size l (dm)**	**Ratio l/D_L**	**U_z (mm)**
Analytic rgdL	$\nu = 0.5$	∞	∞	1.4695
Analytic rgdL	$\nu = 0.49$	∞	∞	1.4889
Analytic P	$\nu = 0.5$	∞	∞	1.8711
Analytic P	$\nu = 0.49$	∞	∞	1.8958
FEM P-Swall	f=1	2	5	1.5919
FEM P-Swall	f=10	20	50	1.8648
FEM rgdL-Swall	f=1	2	5	1.1640
FEM rgdL-Swall	f=1.5	3	7.5	1.2633
FEM rgdL-Swall	f=2	4	10	1.3146
FEM rgdL-Swall	f=3	6	15	1.3660
FEM rgdL-Swall	f=4	8	20	1.3915
FEM rgdL-Swall	f=5	10	25	1.4064
FEM rgdL-Swall	f=6	12	30	1.4162
FEM rgdL-Swall	f=7	14	35	1.4237
FEM rgdL-Swall	f=8	16	40	1.4286
FEM rgdL-Swall	f=9	18	45	1.4323
FEM rgdL-Swall	f=10	20	50	1.4381
FEM rgdL-Swall	f=20	40	100	1.4521
FEM rgdL-Swall	f=50	100	250	1.4594
FEM rgdL-Swall	f=60	120	300	1.4623
FEM rgdL-Swall	f=80	160	400	1.4634
FEM rgdL-Fwall	f=0.5	1	2.5	1.2944
FEM rgdL-Fwall	f=1	2	5	1.3785
FEM rgdL-Fwall	f=1.5	3	7.5	1.4056
FEM rgdL-Fwall	f=2	4	10	1.4217
FEM rgdL-Fwall	f=3	6	15	1.4375
FEM rgdL-Fwall	f=4	8	20	1.4453
FEM rgdL-Fwall	f=6	12	30	1.4521
FEM rgdL-Fwall	f=8	16	40	1.4555
FEM rgdL-Fwall	f=10	20	50	1.4597
FEM rgdL-Fwall	f=20	40	100	1.4628

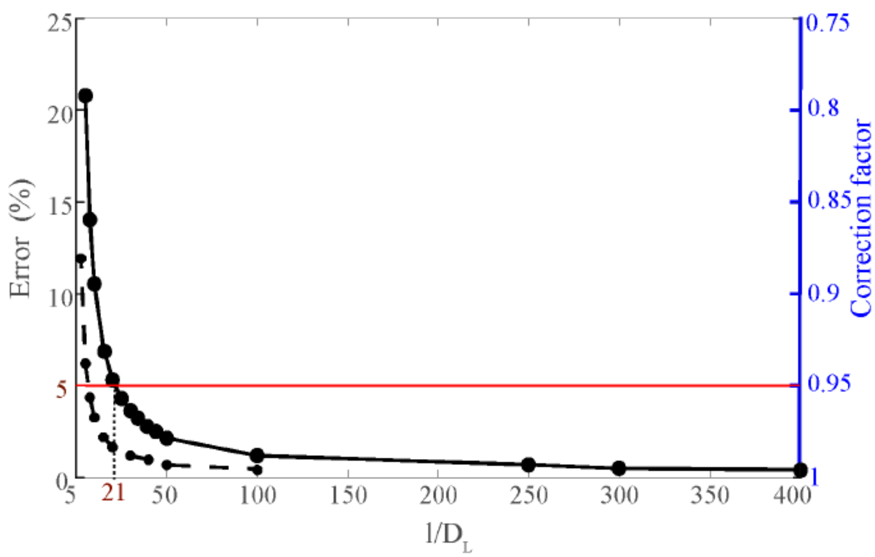

Figure 5: Estimation of the error resulting from the use of the analytical solution for a rigid circular load applied on a half-space (Eq. 5) when estimating the surface displacement induced by a circular load as a function of relative size of the load applied and the tank. The right axis gives the corresponding correction factor to be applied to the value derived analytically in order to obtain the actual value of the Young's modulus inside the tank. The plain and dashed lines are, respectively, for the experimental setup with gelatin adhering to the tank walls and for the case where gelatin is in contact with water on the two proximal lateral sides. Circles indicate the numerical simulations we performed. The red line is for a 5 % error.

of the Young's modulus for each measurement of the vertical displacement. Then for each tank we compute the mean and standard deviation values from all available measurements (Fig. 6 and Tab. 1). For unsalted gelatin at 2 wt %, we estimate $E = 2150 \pm 230$ Pa, with a good reproducibility. Only the first tank (1701) is found to have a lower value $E = 1640$ Pa. However, because neither the length, nor the shape nor the velocity of the cracks in this gelatin block is significantly different from the others, we believe that this low value is due to an error on the measurement of the vertical displacement induced by the load.

Varying gelatin and salt concentration, Young's modulus of salted gelatin range between 300 and 2900 Pa (Tab. 1). As found by Brizzi et al. [24], 2 wt % gelatin with 15 wt % salt has lower Young's modulus than unsalted gelatin at 2 wt %. By increasing the gelatin concentration to 3.5 wt %, we prepared salted gelatin with Young's modulus similar to unsalted gelatin at 2 wt %. We made 3 tanks at 3.5 wt % and 15% salt and we obtain $E = 2065 \pm 120$ Pa, a value close to the Young's modulus estimated for unsalted gelatin at 2 wt %.

4. Comparison of Young's modulus estimates either by shear-wave velocity or surface loading

An alternative method for non-destructive and in-situ measurements of Young's modulus has been proposed recently by Pansino and Taisne [39, 20]. It takes advantage of the birefringent photo-elastic property of the gelatin. This property allows the measurement of the shear wave velocity ν_s and the determination of Young's modulus E^{shw} with the following equation:

$$E^{shw} = 2(1 + \nu)\rho_g \nu_s^2 \tag{8}$$

where ρ_g is the gelatin density and ν is its Poisson's ratio, here, assumed to be 0.5.

Shear wave velocities measurements are performed for 12 gelatin blocks (1 unsalted gelatin and 11 salted gelatin) enabling for a direct comparison with the previous estimates based on surface loading. We compute the Young's modulus E^{shw} for each measured value of shear wave velocity, then we use the mean value and the standard deviation obtained for each gelatin block (Fig. 6 and Tab. 3). Young's modulus estimates using both the surface loading method and the shear wave method have the same order of magnitude.

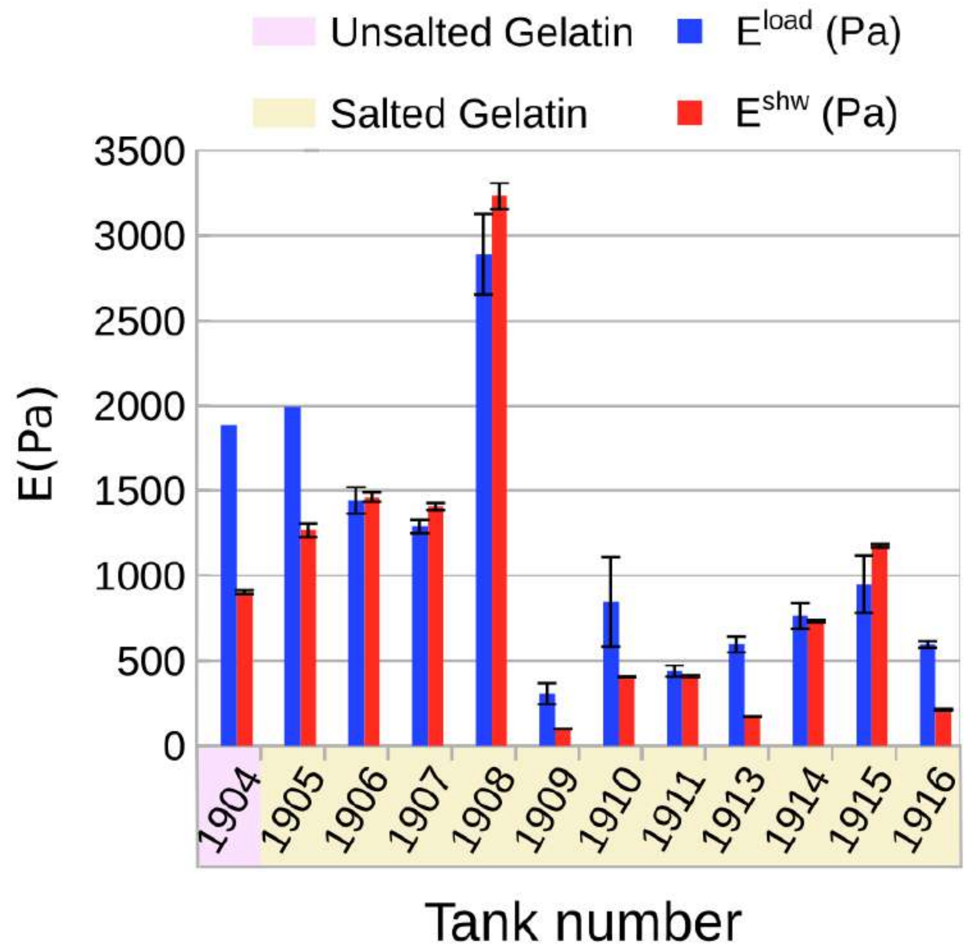

Figure 6: Comparison of Young's Modulus estimated for 12 gelatin tanks and two methods. The average value obtained from several measurements is represented, either derived by the surface loading method (E^{load} in blue), or from shear waves velocity measurements (E^{shw} in red). Tank numbers of unsalted gelatin and salted gelatin are highlighted in purple and orange respectively. Error bars represent the standard deviation.

Table 3: Comparison of Young's modulus estimation by surface loading E^{load} and shear-wave velocity measurement E^{shw} for 12 tanks. ΔE is the absolute difference in Pa, $\frac{\Delta E}{E^{load}}$ is the percentage of difference between both measurements.

Tank	$\mathbf{E^{load}}$ **(Pa)**	$\mathbf{E^{shw}}$ **(Pa)**	$\mathbf{\Delta E}$ **(Pa)**	$\mathbf{\frac{\Delta E}{E^{load}}}$ **(%)**	$\mathbf{\frac{E^{load}}{E^{shw}}}$
1904	1885	905	980	52 %	2.08
1905	1995	1270	725	36 %	1.57
1906	1445	1460	-15	-1 %	1.00
1907	1290	1410	-120	-9 %	0.91
1908	2890	3230	-340	-12 %	0.89
1909	305	100	205	67 %	3.05
1910	845	405	440	52 %	2.09
1911	440	410	30	6 %	1.07
1913	600	170	430	72 %	3.53
1914	760	735	25	3 %	1.03
1915	950	1170	-220	-23 %	0.81
1916	595	210	385	64 %	2.83

Discrepancies over 500 Pa are found only for 2 tanks (1904, 1905) and discrepancies over 60% are found for 3 other tanks (1909, 1913 and 1916) having the smallest values of Young's modulus. In Tab. 3 we report the ratio between E^{load} and E^{shw}, which is smaller in our case (between 0.81 and 3.53) than in Pansino and Taisne [20] (between 0.79 and 5.29). In both studies, a better agreement between estimation by surface loading and by shear waves velocity is observed for more rigid gelatins. Pansino and Taisne [20] attributed the largest values given by the surface loading method to the non homogeneous cooling of the gelatin. Whereas the shear wave method allows to quantify the strength of the interior region of the tank, the surface loading method quantifies the strength of the upper layer, whose hardening by cooling is much quicker than the interior of the tank. This conclusion was supported by larger discrepancy between E^{load} and E^{shw} being observed after a shorter duration of cooling. However, because precise dimension of the load are not provided for each tank of Pansino and Taisne [20]'s study, an overestimation of the Young's modulus by surface loading due to the use of the analytical formula cannot be completely excluded.

5. Young's modulus estimation by crack length measurement

5.1. Principles and theoretical background

The length of propagating air-filled cracks in a gelatin block depends on the injected air volume and on the physical properties of the gelatin [10] such that cracks shape might be used to estimate the Young's modulus [8]. Whereas the critical fluid volume required to ensure a buoyant crack propagation is a function of the fracture toughness [48], the relationship between the injected volume and the crack length only depends on the Young's modulus and buoyancy.

In the framework of the Weertman's theory, a static crack of length $L = 2a$, filled with an incompressible fluid, is characterized by the following half-opening profile w along z direction [49, 50]:

$$w(z) = \frac{1-\nu^2}{E}\Delta\rho g\sqrt{a^2-z^2}(a+z); -a \leq z \leq a, \tag{9}$$

where a is the half-length of the crack and $\Delta\rho = \rho_{solid} - \rho_{fluid}$ is the density contrast between the fluid and the host rock. Integrating the opening profile (Eq. 9) over the crack's length gives the area A of the crack's cross section:

$$A = \frac{\pi(1-\nu^2)}{8}\frac{\Delta\rho g}{E}L^3 \tag{10}$$

The influence of fluid compressibility on Eq. 10 can be shown by using a 2D numerical, boundary-element model (see Fig. 7). In 3D, one could expect for the volume V of the crack :

$$V = \alpha(1-\nu^2)\frac{\Delta\rho g}{E}L^4, \tag{11}$$

with α a constant.

Considering that in side view a rising crack has a shape close to an ellipsoid in its upper part and close to a rectangular in its lower part (Fig. 8a), and that the crack half breadth or lateral dimension r is comprised between $3/4a$ and a [51], it follows that α is expected to range between 0.22 and 0.30.

5.2. Calibration of the Volume-Length relation in 3D

Volumes ranging between 0.4-20 mL were injected with syringes of different sizes (2±0.2, 10±1 or 20±2 mL). Measurements of the crack length from

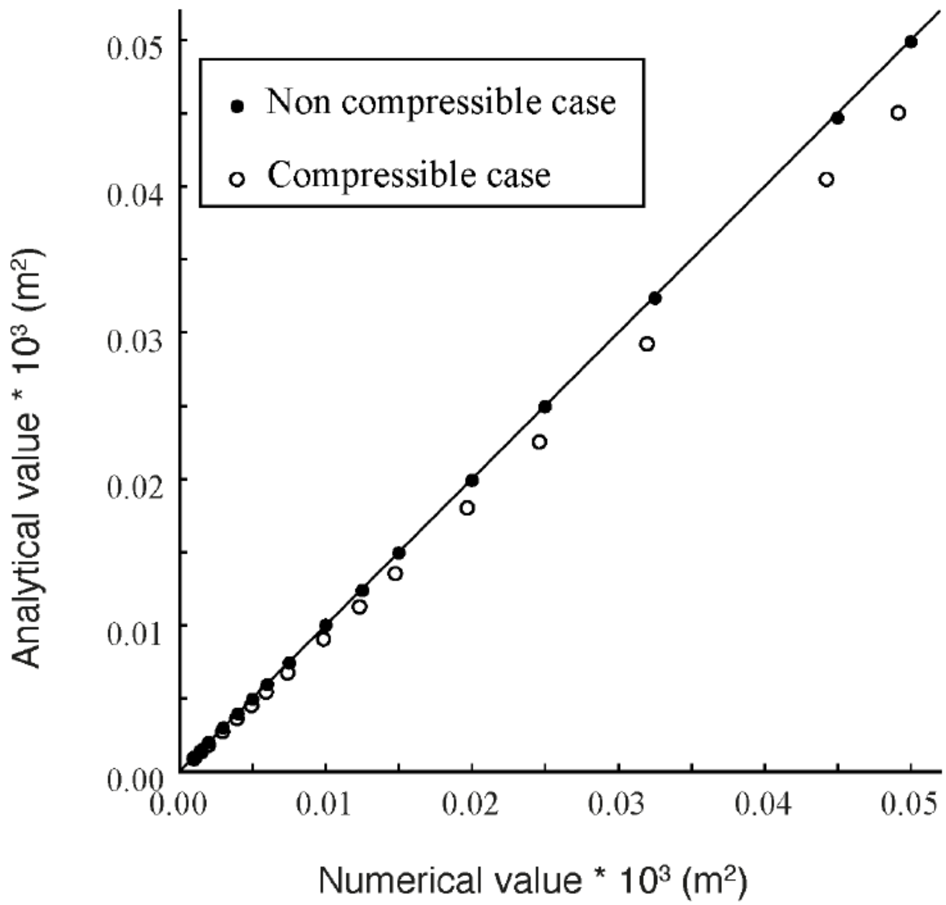

Figure 7: Comparison of the analytical value and the numerical value for the 2D cross-sectional area of a finite length static crack in an infinite elastic medium. Analytical value is given by Eq. 10, the numerical value is calculated with the Boundary Element model described in Maccaferri et al. [52], considering increasing crack lengths. For the compressible case, the bulk modulus of the fluid is set to 100 Pa whereas for the non compressible case it is set to 10^6 Pa.

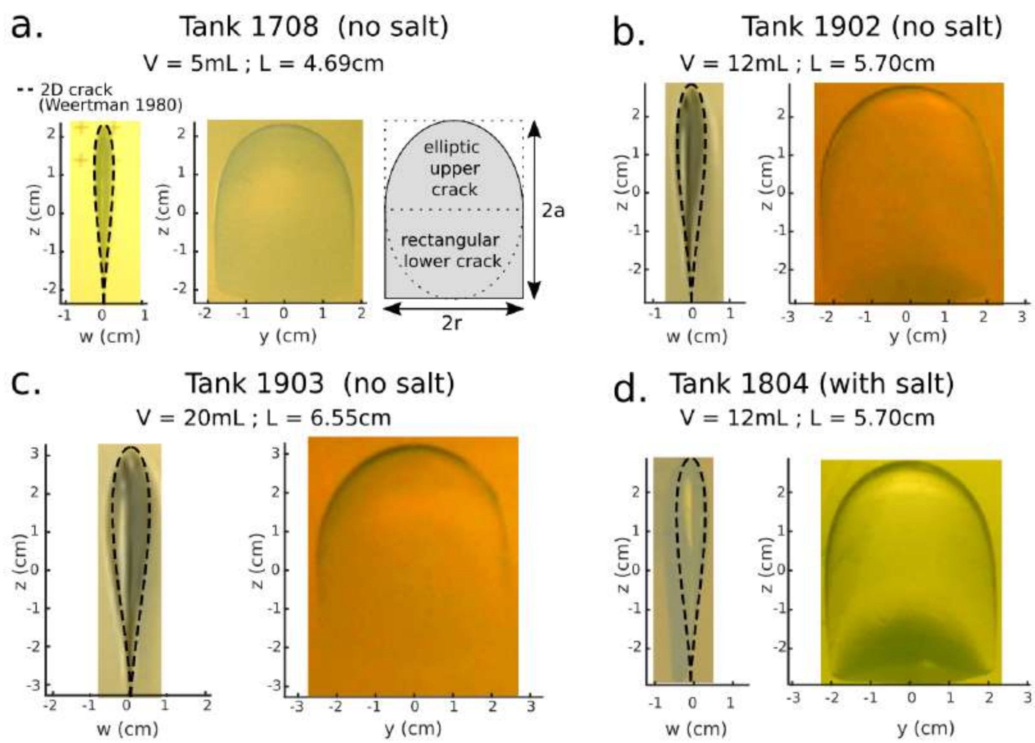

Figure 8: Panels (a), (b), (c) and (d) show crack shapes in cross section (left) and front (right) view of four experiments. Profile opening along cross sections is computed with Eq. 9 (dashed line). Panel (a) also shows a scheme of the theoretical shape of front view as a combination of an elliptic upper part which radius are r (half-width) and a (half-length) and a rectangular lower part which sides are $2r$ and a.

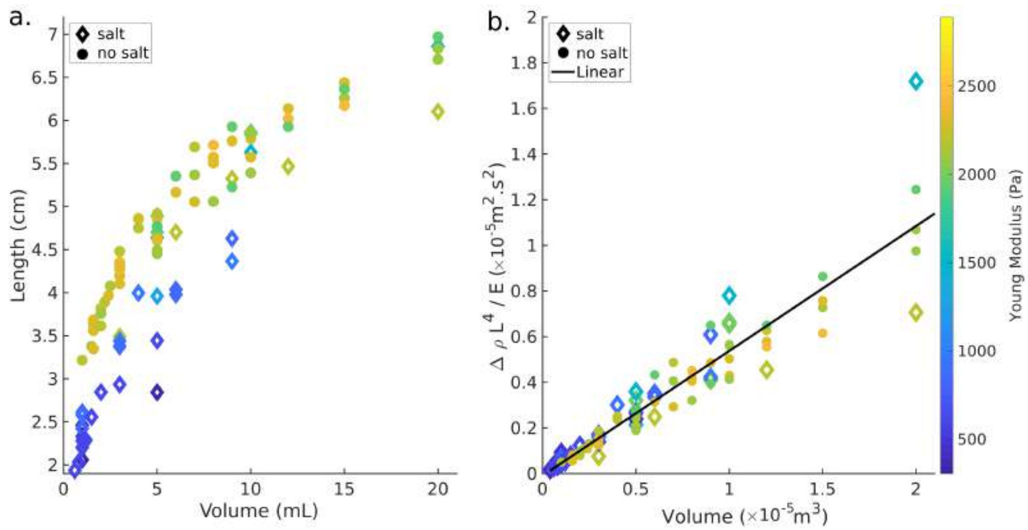

Figure 9: Relationship between crack length (L) and injected volume (V) for air-filled cracks (for all injections performed in tanks 1701 to 1916 listed in Tab. 1). Circles and diamonds represent injections inside unsalted gelatin and salted gelatin, respectively. Colors represent the Young's modulus ($E = E^{load}$) of the tank estimated by surface loading. (a) Crack length (L) as a function of injected volume of air (V). (b) $\frac{\Delta\rho L^4}{E}$ as a function of the injected volume of air (V), the linear tendency gives $\alpha = 0.25$ for Eq. 11.

both cameras are consistent and, for most of the injections, the crack length remains constant during crack propagation.

Fig. 8 shows a selection of cross-section and front views of cracks compared to the opening profile predicted by the Weertman's theory (Eq. 9). As shown by experiments performed injecting 12 mL in tank 1902 (unsalty) and in tank 1804 (salty) which have similar Young's modulus, the crack length is not affected by the addition of salt into the gelatin.

Fig. 9a shows the crack length (L) as a function of the injected volume (V) for each air injection. For a given injected volume, shorter cracks form in gelatin with lower Young's modulus. In order to test the validity of Eq. 11, Fig. 9b represents $\frac{\Delta\rho L^4}{E}$ as a function of the injected volume V. We use our numerically estimated Young's modulus for the first 33 tanks listed in Tab. 1 to calibrate Eq. 11 by determining the proportionality coefficient α. The linear tendency allows to estimate α_{air} to 0.25.

The crack length versus injected volume relationship (Eq. 11 with α_{air} set to 0.25) can thus be used to infer the Young's modulus inside any gelatin tank by measuring the crack length when injecting a known volume of air or of any non-viscous buoyant fluid.

In order to further validate this method, we derive the Young's modulus, from Eq. 11 (E_α) with α=0.25 considering several injected volumes in four tanks (tanks 2002, 2003, 2004 and 2005 as listed in Tab. 1), which were not used to derive α. We then compute the relative differences between E_α and E^{load} (Eq. 12) for several injections (Fig. 10):

$$\frac{\Delta E}{E}(\%) = \frac{|E^{load} - E_\alpha|}{E^{load} + E_\alpha} \times 200 \tag{12}$$

We get a mean error and a standard deviation of 17 $\pm$ 9 % which reflects the dispersion of our data due to measurements uncertainties on length, volume and $\Delta\rho$. Whereas the absolute accuracy of this method does not seem better than 15%, it enables us to evidence potential changes in the Young's modulus along the crack path as discussed below.

5.3. Evidence of a Young's modulus vertical gradient in some experimental tanks

If the Young's modulus of the gelatin tank is homogeneous, the length of the crack does not vary, except in the close vicinity of the upper free surface where it is expected to decrease [53]. Otherwise, a progressive change in the crack length of an ascending crack may reflect a gradient in the rigidity of the gelatin. In two tanks (1806 and 1807), we injected the air a few hours after taking the gelatin out of the fridge. In those cases, cracks are getting shorter and thicker during their ascent consistently with a decrease of the Young's modulus value at shallower depths. In tank 1806, we measure the crack length at several depths for injections 1834 and 1835. Using Eq. 11, we evidence a vertical gradient of rigidity of 35 Pa.cm^{-1} and 43 Pa.cm^{-1}, respectively (Fig. 11).

Those tanks are filled with salted gelatin but the observed gradient cannot originate from a gradient in salt concentration. If it had been the case larger salt concentration would have been expected in the lower part of the gelatin tank resulting in smaller values of Young's modulus at the bottom of the tank. An effect of a gradient in gelatin concentration cannot be excluded, however it is unlikely as such a gradient was never observed in other tanks obtained following the same protocol. Such a decrease of the Young's modulus with decreasing distance to the gelatin surface cannot be due to an ongoing cooling either, as it would result in the reverse gradient. One explanation would be a progressive re-heating of the gelatin tank due to the

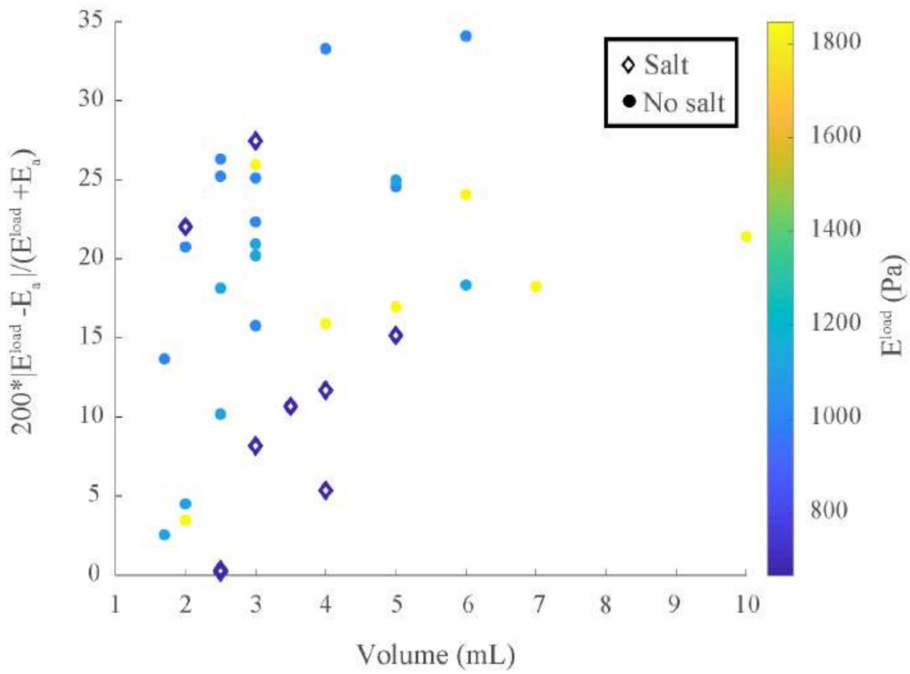

Figure 10: Relative difference between the Young's modulus estimated by air-filled crack length (E_α) and by surface loading (E^{load}) for four tanks (2002, 2003, 2004 and 2005 as listed in Tab 1). Circles and diamonds represent injections inside unsalted gelatin and salted gelatin, respectively. Colors represent the Young's modulus ($E = E^{load}$) of the tank estimated by surface loading. E_α is computed with $\alpha = 0.25$ in Eq. 11.

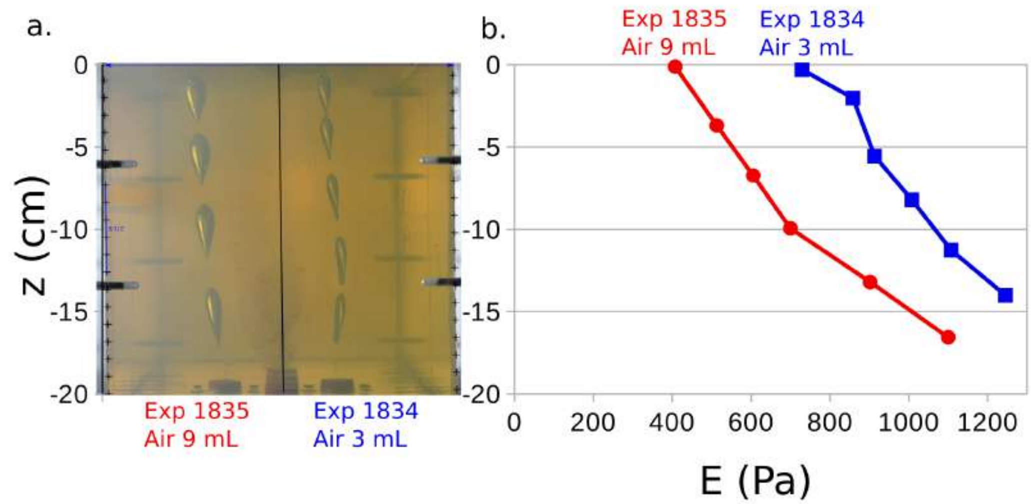

Figure 11: A rigidity gradient affects the tank 1806. (a) Screenshots showing the evolution of the shape of the cracks 1834 (3 mL) and 1835 (9 mL) during propagation. (b) Evolution of E with depth, blue and red curves represent experiments 1834 and 1835 respectively.

lighting. This is consistent with the fact that both experiments were run after a long stay (more than 4 hours) at room temperature. The slightly larger value obtained for the Young's modulus derived from injection 1834, performed before injection 1835, is consistent with this explanation. But the difference between both estimations might also reveal lateral variations in the tank. In particular, the crack in 1835 is injected in the backward side of the tank which is closer to the light source.

6. Fracture toughness characterization

Magma transport through the upper crust occurs mainly by dike propagation. Magma flows inside a planar fracture such that the velocity is partly controlled by fracturing, at least in the tip area, and depends on the crustal fracture toughness [41]. Fracture toughness is thus a key physical parameter of the gelatin for fluid-filled crack propagation experiments. This property is linked to the Young's modulus through the surface energy γ_s (see Eq. 1) [40], which is usually poorly known. Kavanagh et al. [16] estimated the value of surface energy for unsalted gelatin with concentration ranging from 5 to 8 % to be around 1.0 ± 0.2 Jm^{-2}. It was done measuring independently the Young's modulus by surface loading and the fracture toughness by quantifying the pressure required to propagate a pre-existing crack, using a two-dimensional approximation. Here we followed the strategy proposed by Heimpel and Olson [41] to estimate the fracture toughness. We estimated the velocity for several finite size air-filled cracks of various volumes injected inside the same tank of gelatin. We computed the stress intensity factor based on the crack length. Following Secor and Pollard [49], in 2D, the stress intensity factor in mode I K_I^{2D}, for a buoyant crack, can be expressed as:

$$K_I^{2D} = \Delta\rho g a\sqrt{\pi a} \tag{13}$$

Dahm [51] better characterized the 3D shape of buoyancy-driven propagating fractures with an approximately circular and straight line boundary at the upper and lower ends, respectively. He showed that fractures are self similar with the lateral extent (half breadth r) linked to the vertical extent (half length a) by the relationship: $r = (3/4)a$. Using this approximation and the expression for the stress intensity factor in 3D proposed by Heimpel and Olson [41], we can derive a scaling factor between 3D (K_I^{3D}) and 2D (K_I^{2D}) stress intensity factors:

$$K_I^{3D} = \frac{2\sqrt{3}}{\pi}K_I^{2D} = \frac{2\sqrt{3}}{\sqrt{\pi}}\Delta\rho g a\sqrt{a} \approx 1.103K_I^{2D} \tag{14}$$

Fig. 12 shows the evolution of K_I^{3D} as a function of the crack velocity in three different tanks. The critical value for the stress intensity factor is the minimum which allows for crack propagation and equals the fracture toughness of the host medium. Therefore, a linear regression is used to quantify the fracture toughness of the gelatin in each tank, which corresponds to the vertical intercept.

Derived fracture toughness values are listed in Tab. 1 for each tank where this property was estimated. We use our estimates of K_I^{3D}, in combination with estimates of the Young's modulus E^{load}, to compute the surface energy γ_s for our gelatins (Eq. 1). Our results (Fig. 13) are mostly consistent with the previous estimate of γ_s [33, 16]. For unsalted gelatin, we derive a value for γ_s equal to 0.77 Jm^{-2}, which is slighty below the range derived by Kavanagh et al. [16] with more rigid gelatin. Importantly, our results clearly show that, for the same Young's modulus, a salted gelatin is characterized by a higher fracture toughness than an unsalted one. Using all available salted gelatin, for γ_s we obtain a value of 1.32 Jm^{-2}. When omitting tank 1906, which could be considered as an outlier in Fig. 13, we obtain for γ_s a value of 1.10 Jm^{-2}

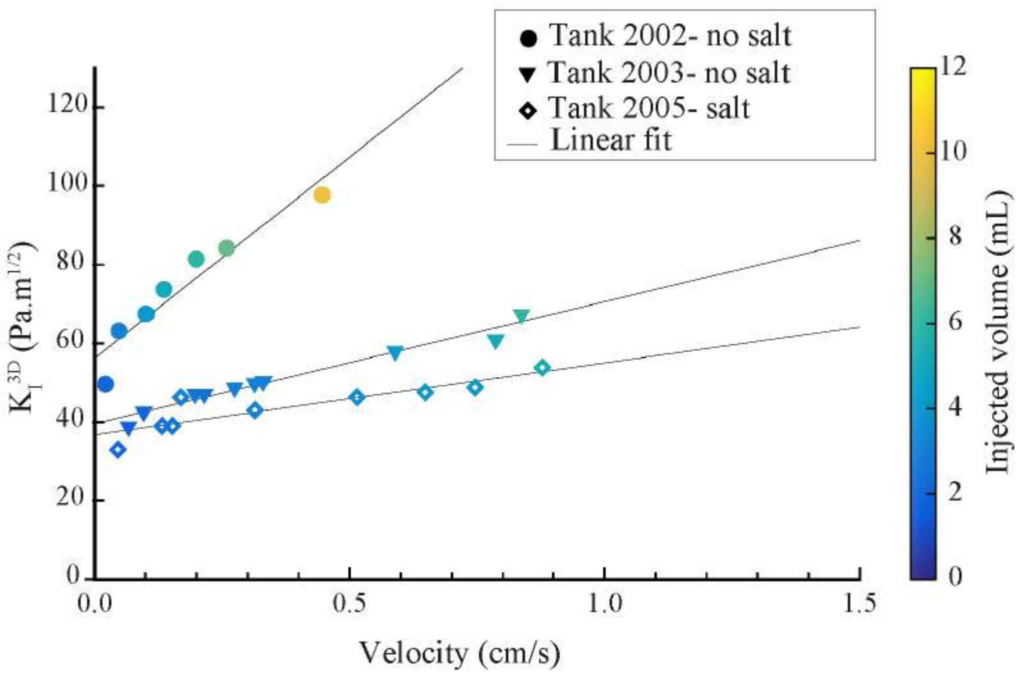

Figure 12: Stress intensity factor K_I^{3D} as a function of vertical velocity. 26 air injections for 3 different tanks (2002 and 2003 unsalted and 2005 salted) are represented. The stress intensity factor is estimated from the 3D theory (Eq. 14). For each tank, the limit of K_I when the vertical velocities tends to zero corresponds to the fracture toughness of the gelatin.

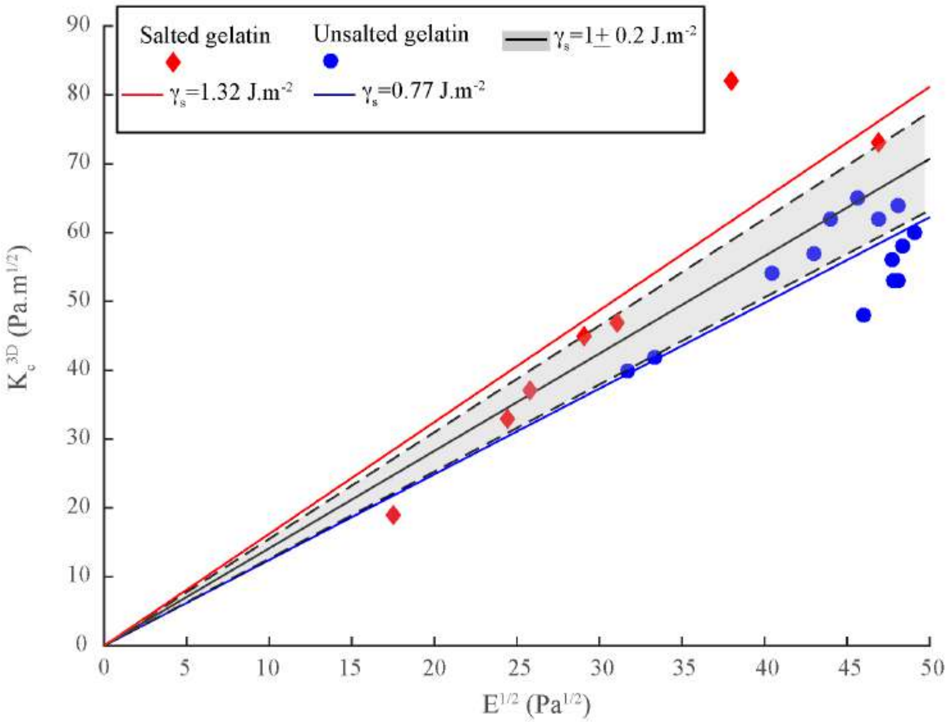

Figure 13: Relationship between the fracture toughness and the Young's modulus. Fracture toughness is estimated using the 3D approximation (Eq. 14). Linear fit, with uncertainties, corresponding to γ_s equal to 1±0.2 Jm^{-2} [33, 16] is represented by the black line, whereas fits obtained from the salted and unsalted tanks are represented, respectively, by red and blue lines.

for the salted gelatin, which is significantly larger than the value obtained for the unsalted one. Further experiments varying the salt concentration would be useful to better characterize the influence of salt on the surface energy of gelatin.

7. Discussion

7.1. Comparison of the various methods for Young's modulus estimation

Our numerical simulations pointed out that the most common method used by experimentalists to infer Young's modulus is reliable (error <5 %) only if the diameter of the load applied at the surface of the gelatin is 20 times smaller than the minimum dimension of the tank. Otherwise, a numerical model is required to link the vertical displacement to the Young's modulus of gelatin taking into account the boundary effect of the rigid tank walls. Here, we also provide a correction factor that can be applied to the value derived from the analytical formula. Even considering the improvement brought by the numerical model, this method still suffers some bias. The major bias is that the measurement is done at the surface, which makes it difficult to reveal potential heterogeneities or layering of the gelatin. The same limitation is encountered when deriving a static value of the crustal Young's modulus from surface loading or unloading events. The lateral extent of the load determines the crustal depth over which the Young's modulus is effectively averaged. In particular, one expects that loads applied on a broader area will probe a thicker layer of the underlying medium. In order to characterize this effect, we perform several numerical simulations in 2D axisymmetry using a FEM. Numerical calculations are performed either to match the experiments (with the Poisson's ratio set to 0.49 and a rigid load applied at the surface) or the crustal Earth case (with the Poisson's ratio set to 0.25 and a uniform pressure applied at the surface). The numerical box size is set to 2000 times the size of the load applied at the surface to match the ideal case of a half-space. We set the Young's modulus to be a linear function of depth at shallow level and constant deeper:

$$\begin{aligned} E(z) = &\quad E_{surf} + \nabla E \times z \text{ for } z < Z_d \\ E(z) = &\quad E_{surf} + \nabla E \times Z_d \text{ for } z \geq Z_d \end{aligned} \tag{15}$$

where E_{surf} is the value of the Young's modulus at the surface (in z=0), ∇E is its vertical gradient and Z_d is the depth at which the Young's modulus becomes constant. The numerical simulation is used to calculate the value of the surface displacement induced by the load. From this value, we can estimate the corresponding Young's modulus (E_{eq}) for a homogeneous medium (using Eq. 5 for the rigid load condition and Eq. 6 for the uniform pressure condition). We then calculate an effective depth Z_{eq} corresponding to the depth over which the actual Young's modulus inside the medium should be averaged in order to obtain E_{eq}. It can be expressed by:

$$Z_{eq} = 2\frac{E_{eq} - E_{surf}}{\nabla E}, \tag{16}$$

providing that Z_{eq} remains smaller than Z_d. Z_{eq} gives an estimate of the penetration depth reached by the surface load for Young's modulus measurements.

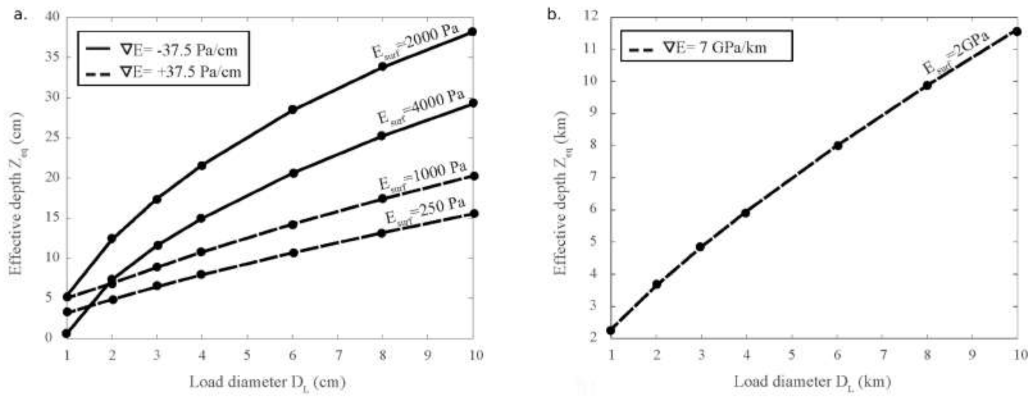

Figure 14: Effective depth over which the Young's modulus is probed as a function of the size of the load applied when there is a vertical gradient. Plain and dashed lines are for a decrease and an increase of the Young's modulus with depth, respectively. Different curves are obtained for various values of the Young's modulus at the surface. Circles are for the numerical simulations performed. a) Cases relevant for the gelatin tank. The depth Z_d at which the Young's modulus becomes constant is here set to 40 cm, the Poisson's ratio to 0.49 and a rigid load is applied at the surface. b) Case relevant for the Earth's crust. The depth Z_d at which the Young's modulus becomes constant is here set to 20 km, the Poisson's ratio to 0.25 and a uniform pressure load is applied at the surface.

Fig. 14 shows Z_{eq} as a function of the size of the load for different Young's modulus profiles. Results are obtained with the depth Z_d set to 40 cm for the experimental case (Fig 14a) and to 20 km for the crustal case (Fig 14b). In all cases, as expected, Z_{eq} increases with the diameter of the load applied. Consequently loads of various diameter might be used to evidence a vertical gradient of the Young's modulus in a gelatin block. In case a load of significant diameter is required, a numerical solution to interpret the subsidence should then be used. Note that applying the load at various location of the tank surface might also be useful to reveal potential lateral gradients. Once again, the use of the numerical model might be necessary.

To infer the gelatin Young's modulus, the alternative method based on the measurement of shear wave velocities as recently proposed by Pansino and Taisne [39, 20] or the new method based on the measurement of the length of a finite volume crack proposed in this study, enable to detect spatial variations of the Young's modulus. They can additionally be used to quantify the potential gradients, which is not possible with surface load measurements. The accuracy of the shear wave velocities method strongly depends on the absolute value of the Young's modulus. Higher rigidity, will produce faster seismic waves, thus reducing the ability to follow a wave train with sufficient resolution before any reflection occurred on the rigid walls. In contrast, the method based on the air-filled crack propagation cannot be considered as strictly non-destructive because once the crack has propagated through it, the gelatin remains cut along the path followed by the crack.

Going back to the Earth's crust, seismic tomography has been used to infer spatial variations of the Young's modulus at depth, usually showing an increase of the rigidity with depth [54, 29, 30], whereas measurements made by surface loading or unloading only provide a value averaged over a given crustal thickness below the surface. Fig. 14b presents the depth probed by surface loading as a function of the lateral extent of the load for values corresponding to a typical crust. Note that usually when using surface displacements induced by surface loading to infer the crustal rheology, the load size is imposed by the natural phenomenon at play (e.g. lake level change, ice thickness variations, etc.). Also, similarly to what we propose for the gelatin, the length of magma intrusions could potentially be used to bring insight into the crustal Young's modulus. However it might be difficult to have a precise knowledge of the volume of magma involved. Besides, here we derived the relationship between length and volume for a non viscous fluid, which might be not fully appropriate in case of dynamic magma propagation.

7.2. Critical length for crack propagation

The critical volume required to ensure liquid-filled fracture propagation is key information both in the hydraulic fracturing domain and in volcanology. Using a numerical model and analytical derivation, Davis et al. [48] and Salimzadeh et al. [55] provided an expression for the critical volume for vertical propagation of a buoyant crack in three dimensions. They underlined that previous estimations for critical "volumes" were only given in terms of critical fracture length and based on analyses performed in 2-D. In particular, following Secor and Pollard [49] and using the fact that the stress intensity factor is equal to the fracture toughness at the upper tip and zero at the lower tip of the crack, the critical half-length is given by:

$$a_c = \left(\frac{K_c}{\Delta\rho g \sqrt{\pi}} \right)^{2/3}, \tag{17}$$

Using again the approximation $r = (3/4)a$ and the expression for the stress intensity factor in 3D proposed by Heimpel and Olson [41], we end up with an expression for the critical length in 3D:

$$a_c = \left(\frac{\sqrt{\pi}}{2\sqrt{3}} \frac{K_c}{\Delta\rho g} \right)^{2/3}, \tag{18}$$

Using Eq. 18 and Eq. 11, we obtain an expression for the critical volume and can express it the same way used by Davis et al. [48]. Using α equal to 0.25 in Eq. 11, we have:

$$V_c = \alpha \frac{2^{13/3}}{9} \frac{1-\nu}{16\mu} \left(\frac{9\pi^4 K_c^8}{\Delta\rho^5 g^5} \right)^{1/3}, \tag{19}$$

$$V_c \approx 0.56 \frac{1-\nu}{16\mu} \left(\frac{9\pi^4 K_c^8}{\Delta\rho^5 g^5} \right)^{1/3}, \tag{20}$$

with μ the shear modulus. Eq. 20 is very close to the expression numerically derived by Davis et al. [48], who gave a coefficient of 0.75 instead of 0.56. This expression of the critical volume can be useful to interpret the volume of magmatic dikes keeping in mind that it was derived neglecting potential viscous effects.

7.3. Young's modulus decrease and surface energy increase in presence of salt

We used the independent estimation of Young's modulus and fracture toughness to estimate the surface energy of the gelatin. We evidenced that the surface energy is increased by addition of salt. It follows that for the same value of the Young's modulus, a salted gelatin will have a higher fracture toughness. This is consistent with the roughly six times higher velocity measured in unsalted gelatin, for a similar injected volume and a similar Young's modulus (Fig. 8). In the same way the critical volume for crack propagation is larger for the salted gelatin than for the unsalted one. It is thus important to take into account this influence of the salt on the surface energy of the gelatin when using salted gelatin as a crustal analog. In particular, to enable the injection of viscous fluids like vegetable or silicon oils, the use of salted gelatin might be required in order to guarantee a sufficient buoyancy. In this case, the fracture toughness cannot be simply derived using the surface energy for unsalted gelatin.

8. Conclusion

We illustrated the added value of using numerical simulations to improve the interpretation of analog experiments. In particular, we quantified the errors associated with the use of the analytical formula corresponding to an elastic half-space [45] for a finite medium. An overestimation of 5 % is expected when using this analytical formula to derive the Young's modulus if the tank size is not 20 times larger than the load diameter when a standard experimental setup is used with gelatin adhering to the tank walls. We showed that using a 3D numerical model removes the constraint of only applying surface loads of limited diameters to derive the Young's modulus. This enables, for instance, to check for potential heterogeneous elastic properties inside a gelatin tank. Two others methods are suitable to quantify the Young's modulus and can alternatively reveal its variations inside a tank. One consists of measuring shear wave velocities, which is fully non-destructive. The other is based on the calibration performed in this study and requires the quantification of the length of cracks filled with a known volume of a non-viscous buoyant fluid, which can be done with limited alteration of the gelatin. In addition we highlighted the influence of salt on gelatin physical properties. While salt was known to decrease the Young's modulus value of the gelatin, we showed that it also increases its surface energy. More generally, the information provided by numerical models regarding the depth probed by surface loading, might prove to be useful when interpreting Young's modulus values for the Earth's crust derived by static loading/unloading events. Based on our numerical model results in the case of a linear increase of the crustal Young's modulus with depth, we confirm that the lateral size of the surface loading (or unloading) considered should be the same order of magnitude as the crustal thickness to be probed.

Acknowledgements

We thank Jacques Grangeon for his technical support on the experimental work carried out in Chambery. Tim Davis, Medhi Nikhoo, Ayleen Gaete, Sreeram Reddy Kotha and Nima Nooshiri for their support on the experimental work carried out in Potsdam and nice discussions on gelatin experiments and dike propagation. We thank the Editor—Philippe Agard— and the reviewers—Simon Martin and Steve Pansino—for their constructive comments. Open source softwares used in this study are available here :

https://physlets.org/tracker and https://shotcut.org. We also used the commercial modeling software COMSOL : https://www.comsol.fr.

Fundings

This work received financial support from the ANR-DFG NLE 2018 MagmaPropagator projet (ANR-18-CE92-0037), from the German Academic exchange Sercice (DAAD) through the Research Grants - Short-Term Grants, 2019 (57440917) and from ISTerre (BQR project funded in 2020). ER was funded by the Deutsche Forschungsgemeinschaft (DFG – German Research Foundation), Grant RI 2782/2-1.

References

[1] E. Di Giuseppe, F. Funiciello, F. Corbi, G. Ranalli, G. Mojoli, Gelatins as rock analogs: A systematic study of their rheological and physical properties, Tectonophysics 473 (2009) 391–403.

[2] J. E. Reber, M. L. Cooke, T. P. Dooley, What model material to use? a review on rock analogs for structural geology and tectonics, Earth-Science Reviews 202 (2020) 103107. doi:https://doi.org/10.1016/j.earscirev.2020.103107.

[3] F. Corbi, F. Funiciello, M. Moroni, Y. Van Dinther, P. M. Mai, L. Dalguer, C. Faccenna, The seismic cycle at subduction thrusts: 1. insights from laboratory models, Journal of Geophysical Research: Solid Earth 118 (2013) 1483–1501.

[4] P. McLeod, S. Tait, The growth of dykes from magma chambers, Journal of Volcanology and Geothermal Research 92 (1999) 231–246.

[5] E. Canon-Tapia, O. Merle, Dyke nucleation and early growth from pressurized magma chambers: Insights from analogue models, Journal of volcanology and geothermal research 158 (2006) 207–220.

[6] F. Manta, A. Emadzadeh, B. Taisne, New insight into a volcanic system: Analogue investigation of bubble-driven deformation in an elastic conduit, Journal of Geophysical Research: Solid Earth 124 (2019) 11274–11289.

[7] R. Fiske, E. Jackson, Orientation and growth of hawaiian volcanic rifts: the effect of regional structure and gravitational stresses, Proceedings of the Royal Society of London. A. Mathematical and Physical Sciences 329 (1972) 299–326.

[8] A. Takada, Experimental study on propagation of liquid-filled crack in gelatin: Shape and velocity in hydrostatic stress condition, Journal of Geophysical Research: Solid Earth 95 (1990) 8471–8481.

[9] J. R. Muller, G. Ito, S. J. Martel, Effects of volcano loading on dike propagation in an elastic half-space, ournal of Geophysical Research: Solid Earth 106 (2001) 11,101–11,113.

[10] E. Rivalta, M. Böttinger, T. Dahm, Buoyancy-driven fracture ascent: Experiments in layered gelatine, Journal of Volcanology and Geothermal Research 144 (2005) 273–285.

[11] T. Menand, K. Daniels, P. Benghiat, Dyke propagation and sill formation in a compressive tectonic environment, Journal of Geophysical Research: Solid Earth 115 (2010).

[12] J. L. Kavanagh, A. J. Burns, S. H. Hazim, E. P. Wood, S. A. Martin, S. Hignett, D. J. Dennis, Challenging dyke ascent models using novel laboratory experiments: Implications for reinterpreting evidence of magma ascent and volcanism, Journal of Volcanology and Geothermal Research 354 (2018) 87–101.

[13] F. Maccaferri, D. Smittarello, V. Pinel, V. Cayol, On the Propagation Path of Magma-Filled Dikes and Hydrofractures: The Competition Between External Stress, Internal Pressure, and Crack Length, Geochemistry, Geophysics, Geosystems (2019).

[14] M. Hubbert, Theory of scale models as applied to the study of geologic structures, Bulletin of the Geological Society of America 48 (1937) 1,459–1,517.

[15] J. van Otterloo, A. R. Cruden, Rheology of pig skin gelatine: Defining the elastic domain and its thermal and mechanical properties for geological analogue experiment applications, Tectonophysics 683 (2016) 86–97.

[16] J. Kavanagh, T. Menand, K. A. Daniels, Gelatine as a crustal analogue: Determining elastic properties for modelling magmatic intrusions, Tectonophysics 582 (2013) 101–111.

[17] M. Czerner, L. A. Fasce, J. F. Martucci, R. Ruseckaite, P. M. Frontini, Deformation and fracture behavior of physical gelatin gel systems, Food Hydrocolloids 60 (2016) 299–307.

[18] F. Farquharson, R. G. Hennes, Gelatin models for photoelastic analysis of stress in Earth masses, Civil Engineering 10 (1940) 211–214.

[19] J. D. Crisp, The use of gelatin models in structural analysis, Proceedings of the Institution of Mechanical Engineers 167 (1953) 580–604.

[20] S. Pansino, B. Taisne, Shear wave measurements of a gelatin's young's modulus, Frontiers in Earth Science 8 (2020) 171.

[21] V. Acocella, A. Tibaldi, Dike propagation driven by volcano collapse: a general model tested at Stromboli, Italy, Geophysical Research Letters 32 (2005).

[22] J. L. Kavanagh, T. Menand, R. S. J. Sparks, An experimental investigation of sill formation and propagation in layered elastic media, Earth and Planetary Science Letters 245 (2006) 799–813.

[23] M. C. Ritter, V. Acocella, J. Ruch, S. L. Philipp, Conditions and threshold for magma transfer in the layered upper crust: Insights from experimental models, Geophysical Research Letters 40 (2013) 6043–6047.

[24] S. Brizzi, F. Funiciello, F. Corbi, E. Di Giuseppe, G. Mojoli, Salt matters: How salt affects the rheological and physical properties of gelatine for analogue modelling, Tectonophysics 679 (2016) 88–101.

[25] M. J. Heap, M. Villeneuve, F. Albino, J. I. Farquharson, E. Brothelande, F. Amelung, J.-L. Got, P. Baud, Towards more realistic values of elastic moduli for volcano modelling, Journal of Volcanology and Geothermal Research 390 (2020) 106684.

[26] F. Beauducel, F.-H. Cornet, E. Suhanto, T. Duquesnoy, M. Kasser, Constraints on magma flux from displacements data at Merapi volcano, Java, Indonesia, Journal of Geophysical Research: Solid Earth 105 (2000) 8,193–8,203.

[27] R. Grapenthin, F. Sigmundsson, H. Geirsson, T. Arnadóttir, V. Pinel, Icelandic rhythmics: Annual modulation of land elevation and plate spreading by snow load, Geophysical Research Letters 33 (2006).

[28] V. Pinel, F. Sigmundsson, E. Sturkell, H. Geirsson, P. Einarsson, M. Gudmundsson, T. Högnadóttir, Discriminating volcano deformation due to magma movements and variable surface loads: application to Katla subglacial volcano, Iceland, Geophysical Journal International 169 (2007) 325–338.

[29] G. Currenti, C. Del Negro, G. Ganci, Modelling of ground deformation and gravity fields using finite element method: an application to Etna volcano, Geophysical Journal International 169 (2007) 775–786.

[30] C. Wauthier, V. Cayol, F. Kervyn, N. d'Oreye, Magma sources involved in the 2002 Nyiragongo eruption, as inferred from an InSAR analysis, Journal of Geophysical Research: Solid Earth 117 (2012).

[31] C. H. Cheng, D. H. Johnson, Dynamic and static moduli, Geophysical Research Letters 8 (1981) 39–42.

[32] M. Adelinet, J. Fortin, Y. Guéguen, A. Schubnel, L. Geoffroy, Frequency and fluid effects on elastic properties of basalt: Experimental investigations, Geophysical Research Letters 37 (2010).

[33] T. Menand, S. R. Tait, The propagation of a buoyant liquid-filled fissure from a source under constant pressure: An experimental approach, Journal of Geophysical Research: Solid Earth 107 (2002) ECV–16.

[34] K. A. Daniels, T. Menand, An experimental investigation of dyke injection under regional extensional stress, Journal of Geophysical Research: Solid Earth 120 (2015) 2014–2035.

[35] A. Gaete, J. L. Kavanagh, E. Rivalta, S. H. Hazim, T. R. Walter, D. J. Dennis, The impact of unloading stresses on post-caldera magma intrusions, Earth and Planetary Science Letters 508 (2019) 109–121.

[36] F. Corbi, E. Rivalta, V. Pinel, F. Maccaferri, V. Acocella, Understanding the link between circumferential dikes and eruptive fissures around calderas based on numerical and analog models, Geophysical Research Letters 43 (2016) 6212–6219.

[37] V. Pinel, A. Carrara, F. Maccaferri, E. Rivalta, F. Corbi, A two-step model for dynamical dike propagation in two dimensions: Application to the july 2001 etna eruption, Journal of Geophysical Research: Solid Earth 122 (2017) 1107–1125.

[38] T. Watanabe, T. Masuyama, K. Nagaoka, T. Tahara, Analog experiments on magma-filled cracks: Competition between external stresses and internal pressure, Earth and Planetary Science Letters 54 (2002) 1,247–1,261.

[39] S. Pansino, B. Taisne, How Magmatic Storage Regions Attract and Repel Propagating Dikes, Journal of Geophysical Research: Solid Earth 124 (2019) 274–290.

[40] A. Griffith, The phenomena of rupture and flow in solids., Philosophical transactions of the Royal Society of London. Series A: Mathematical and physical sciences 221 (1921) 163–198.

[41] M. Heimpel, P. Olson, Buoyancy-driven fracture and magma transport through the lithosphere: models and experiments, Internation Geophysics 57 (1994) 223–240.

[42] T. Heycke, L. Spitzer, Screen recordings as a tool to document computer assisted data collection procedures, Psychologica Belgica 59 (2019) 269.

[43] C. Multiphysics, Introduction to comsol multiphysics®, COMSOL Multiphysics, Burlington, MA, accessed Feb 9 (1998) 2018.

[44] N. Le Corvec, T. Menand, J. Lindsay, Interaction of ascending magma with pre-existing crustal fractures in monogenetic basaltic volcanism: an experimental approach, Journal of Geophysical Research: Solid Earth 118 (2013) 968–984. doi:10.1002/jgrb.50142.

[45] S. Timoshenko, J. N. Goodier, H. N. Abramson, Theory of elasticity, Journal of Applied Mechanics 37 (1970) 888.

[46] I. N. Sneddon, Fourier Transforms McGraw-Hill Book Co, Inc., New York (1951).

[47] F. Sigmundsson, P. Einarsson, Glacio-isostatic crustal movements caused by historical volume change of the Vatnajökull ice cap, Iceland, Geophysical Research Letters 19 (1992) 2123–2126.

[48] T. Davis, E. Rivalta, T. Dahm, Critical fluid injection volumes for uncontrolled fracture ascent, Geophysical Research Letters 47 (2020) e2020GL087774.

[49] D. T. Secor, D. D. Pollard, On the stability of open hydraulic fractures in the Earth's crust, Geophysical Research Letters 2 (1975) 510–513.

[50] J. Weertman, The stopping of a rising liquid-filled crack in the Earth's crust by a freely sleeping horizontal joint, Journal of Geophysical Research: Solid Earth 85 (1980) 967–976.

[51] T. Dahm, On the shape and velocity of fluid-filled fractures in the earth, Geophysical Journal International 142 (2000) 181–192.

[52] F. Maccaferri, M. Bonafede, E. Rivalta, A quantitative study of the mechanisms governing dike propagation, dike arrest and sill formation, Journal of Volcanology and Geothermal Research 208 (2011) 39–50.

[53] E. Rivalta, T. Dahm, Acceleration of buoyancy-driven fractures and magmatic dikes beneath the free surface, Geophysical Journal International 166 (2006) 1,424–1,439.

[54] A. Gudmundsson, Effect of tensile stress concentration around magma chambers on intrusion and extrusion frequencies, Journal of Volcanology and Geothermal Research 35 (1988) 179–194.

[55] S. Salimzadeh, R. W. Zimmerman, N. Khalili, Gravity hydraulic fracturing: A method to create self-driven fractures, Geophysical Research Letters 47 (2020) e2020GL087563.